Master's thesis

NTNU
Norwegian University of Science and Technology
Faculty of Engineering
Department of Manufacturing and Civil Engineering

Robert William Rolle

Gap Tolerance for Friction Stir Welding of Large, Extruded Aluminum Profiles

Master's thesis in Sustainable Manufacturing
Supervisor: Geir Ringen
June 2022

NTNU
Norwegian University of Science and Technology

Robert William Rolle

Gap Tolerance for Friction Stir Welding of Large, Extruded Aluminum Profiles

Master's thesis in Sustainable Manufacturing
Supervisor: Geir Ringen
June 2022

Norwegian University of Science and Technology
Faculty of Engineering
Department of Manufacturing and Civil Engineering

NTNU
Norwegian University of
Science and Technology

Abstract

Friction stir welding is a method of joining materials, such as aluminum, without the use of consumable tools or an external heat source. The present work has investigated how robust the friction stir welding process is when encountering gaps due to improper fitting workpieces. The experiment conducted in this study is focused on welding hollow extruded 6082-T6 aluminum profiles, of 1-meter length, with designed gap spacings created between them. The profiles which were assessed have weld thicknesses of 17 mm and 23 mm on either side. A gapless weld was performed as a baseline to compare the designed gaps of 0.0, 1.0, 1.5, 2.0, and 3.0 mm. To further examine the results of the testing the forces and torque of the weld have been analyzed and discussed, a macrographic examination of the welds was performed, and tensile tests were performed on the last half of the weld. This was a preliminary study into how the friction stir welding process performs with welds of these thicknesses on hollow extruded profiles.

The results from this study show that the welding process is able to produce sound welds, at both weld thicknesses, for the 2.0 mm gap and below. At the 3.0 mm gap level, voids are present on the advancing side of the nugget zone within the weld. There is also evidence, within the macrographic examination, of a lack of friction-produced heat as the thermo-mechanically affected zone is severely reduced on the advancing side when the voids are present. The tensile test results show that the ultimate tensile strength of the gapped welds is reduced minimally when compared with the baseline gapless weld. At both the 17 mm and 23 mm weld thickness, all gap levels stayed within 1.22% of the ultimate tensile strength of the gapless welds.

Sammendrag

Friksjonssveising er en metode for sammenføyning av materialer, som aluminium, uten bruk av tilsatsmateriale eller en ekstern varmekilde. Denne studien har undersøkt hvor robust friksjonssveiseprosessen er ved varierende gap på grunn av geometrivariasjon og/eller nøyaktighet ved klamping. Eksperimentet i denne studien baseres på sammenføyning av 6082-T6 aluminium hulsprofiler, lengde på 1 meter, med manipulerte gapavstander mellom profilene. Aluminiumsprofilene har sveisetykkelser fra 17 mm til 23 mm på hver side. En gapløs sveis ble utført som et basiseksperiment og sammenligningsgrunnlag for eksperimenter med gap fra 0,0, 1,0, 1,5, 2,0 og 3,0 mm. For å analysere resultatene, er kraft, moment, rotasjonshastighet og sveisehastighet målt i prosessen, samt at makrografiske undersøkelser av sveisene er utført sammen med strekktester. Denne studien er å anse som en forstudie av hvordan friksjonsrørsveiseprosessen fungerer for sammenføyning av relativt tykke sveiser av hulprofiler med økende sveisegap.

Resultatene fra denne studien viser at sveiseprosessen er i stand til å produsere gode sveiser, ved begge sveisetykkelser, for mindre enn 2,0 mm gap. Ved 3,0 mm gapnivå oppstår et hulrom på den fremadskridende siden av nugget-sonen i sveisen. Det er også bevist med makrografiske undersøkelser, mangel på friksjonsvarme siden den termomekanisk påvirkede sonen er sterkt redusert på den fremadskridende siden når hulrommet oppstår. Strekktestresultatene viser at den ultimate strekkfastheten til sveisene reduseres minimalt sammenlignet med den grunnleggende gapfrie-sveisen. Ved både 17 mm og 23 mm sveisetykkelse holdt alle gapnivåer seg innenfor 1,22 % av den endelige strekkstyrken til de gapfrie sveisene.

Preface

I would like to thank my supervisor Geir Ringen for all of the contacts and guidance during the many moving parts of the experimental work during this thesis. I would also like to thank Harald Vestøl for all of the organization and support during the course of the thesis. Further, thank you to Lise Sandnes for organizing, guiding, and giving insight during the tensile testing.

Thank you to everyone at Hydro Extrusions Innovation & Technology for the use of the welding machine, laboratory, and for welcoming me to Sweden. A special thank you to Jan Backlund for your time and effort in the laboratory and for sharing your expertise on friction stir welding.

Lastly, I would like to thank everyone else who was involved in any way along the course of this thesis.

Table of Contents

List of Figures

List of Tables

List of Abbreviations (or Symbols)

GMAW	Gas Metal Arc Welding
FSW	Friction Stir Welding
Si	Silicon
Mg	Magnesium
UTS	Ultimate Tensile Strength
MPa	Megapascal
CD	Circumscribing Circle Diameter
AS	Advancing Side
RS	Retreating Side
NZ	Nugget Zone
TMAZ	Thermo-mechanically Affected Zone
HAZ	Heat Affected Zone
VCFSW	Vertical Compensation Friction Stir Welding
Nm	Newton meter
kN	Kilonewton

1 Introduction

1.1 Background

Aluminum is an exceptionally durable metal with a high strength-to-weight ratio, making it a convincing material choice with regard to its usefulness in a variety of industrial settings. It is also a particularly good material in terms of sustainability. The light-weight properties of aluminum allows for less consumption of energy during the use of products where weight savings are essential, such as automobiles and airplanes. The natural formation of oxide film on the surface of aluminum provides good performance in corrosive environments without the need for coatings and can reduce maintenance expenses [1]. Also, aluminum can be remelted and recycled into new products numerous times, with only minimal metal losses each time, while also saving approximately 95% of the energy use compared to making new metal from bauxite ore [2]. Although, because it is so highly durable almost 75% of all aluminum ever produced is still in use and has not become available for recycling [3].

In 2021 there were 67 000 thousand metric tonnes of aluminum produced globally, with China leading strongly with 57.8% of production, followed by Gulf Cooperation Council (8.8%), and Asia excluding China (6.7%) [4]. Nearly all branches of global industry consume aluminum, including: defense industry, aircraft engineering, shipbuilding, power production industry, and fabrication of construction materials [5]. The use of aluminum in the construction industry has grown heavily in recent years, and now stands as the largest aluminum consuming sector, with 25% of global end use of aluminum products as of 2020 [6]. This can be attributed to the material's properties, as mentioned above, but also because of its relative ease of manufacture. Aluminum alloy can be extruded and rolled formed to a broad range of cross-sectional shapes, enabling aluminum alloy to be used efficiently under a wide variety of loading conditions [7]. The extrusion process makes it possible to improve the geometrical properties of the cross-section by designing a shape which simultaneously gives minimum weight and highest structural efficiency. Obtaining these stiffened shapes without using built-up sections can avoid the need for welding, bolting, or other joining operations [1].

There are many cases where aluminum will need to be joined and this can be done by adhesives, mechanical fasteners such as rivets, and most aluminums can be welded by conventional methods such as gas metal arc welding (GMAW). When joining aluminum through welding operations, some of the perceived benefits of the material can turn into an obstacle to overcome. The aforementioned oxide layer, which develops naturally, must be cleaned mechanically or chemically to remove the heavy oxides which will impair welding if not minimized [8]. Thermal conductivity is the physical property which affects weldability the most in aluminum. The thermal conductivity of aluminum is four times that of low-carbon steel, meaning that heat must be applied four times as fast to aluminum alloys as to steel to raise the temperature locally by the same amount [8].

Friction stir welding (FSW), the focal process of this thesis, can alleviate some of the issues which are common in fusion welding. FSW is performed below the melting temperature of the material, which minimizes some typical defects encountered in fusion welding such as

cracking, porosity and alloying element loss [9]. The FSW process is capable of absorbing small fit-up type variations without a noticeable effect on tensile strength [10]. However, because there is typically no filler material added during the process, the FSW process will struggle when larger gaps or misalignments are present between the parts which will be joined. The plasticized material may escape in the presence of a gap, or the weld may become too thin due to the lack of material to fill the void. Ideally material preparation prior to FSW is targeted to ensure good fit-up, realistically, certain manufacturing processes, such as extrusion, impart dimensional variations that must be accommodated for the application of FSW in a production environment [11].

1.2 Objective and scope

In the search for literature regarding FSW in the presence of a gap, it was found that there is limitations to the thicknesses of material which have been investigated and experimented with. Nearly all of the studies identified have experimented with material in the range of 4-7 mm wall thickness in the form of butt welding of basic flat plates. As mentioned in the previous section, the construction industry is currently the largest consumer of global end of use products. When discussing structural, load bearing aluminum components such as beams or girders, the material thicknesses involved will be required to be much higher and the geometries more complex. The forces that hollow and complex geometries will experience during FSW are likely to have a different effect on the outcome of the weld then would be experienced when joining flat plates.

This study aims to identify the allowable gap tolerance for FSW of extruded aluminum profiles of 17- and 23-mm wall thickness. These profiles are part of an ongoing concept for an aluminum suspension bridge which is anticipated to be built over the Langenuen fjord. In commercial use it is natural, and expected, that extruded aluminum profiles will have some identifiable deviations from nominal form and dimensional values due to the heating, high pressure extrusion, and rapid cooling involved in the process. As the length of extrusion becomes longer, the straightness of the profiles is likely to suffer. The forces from the FSW fixture's clamping system can alleviate this issue to a degree, however some gaps are still likely to be encountered. Through experimentation involving FSW of designed gaps, visual inspection through macrographic examination, and tensile testing this thesis is a preliminary investigation towards how stable the FSW process is when encountering gaps for higher thickness welds. This study can be used a starting point for future works and research regarding the effectiveness of the FSW process with regard to gaps and misalignments while welding aluminum profiles of high wall thickness and hollow geometry.

2 Theory

This chapter presents theoretical knowledge regarding the topics of this thesis. Within are detailed information about aluminum, the characteristics of the 6xxx series alloys, and the extrusion process. After this, information regarding the Langenuen Bridge and specifically the profiles which this thesis involves for experimentation. To end this chapter are knowledge about the FSW process and a literature review regarding current knowledge about gap tolerances in FSW.

2.1 Aluminum

2.1.1 Aluminum production

Bauxite, a mixture of aluminum oxides, iron oxides, and clay is the principal aluminum-containing ore for the commercial production of aluminum metal [12, 13]. Most bauxite production comes from surficial deposits which formed in tropical or subtropical environments, located in areas which are comparatively stable tectonically [14]. In 2018, global production of bauxite was 335 million tonnes with Australia (29%) as the leading producer followed by China (21%) and Guinea (18%) [12]. Production of aluminum metal from bauxite is a two-stage process. The first stage, the Bayer Process, involves the refining of bauxite ore, resulting in the production of pure alumina [14], as can be seen in Figure 1.

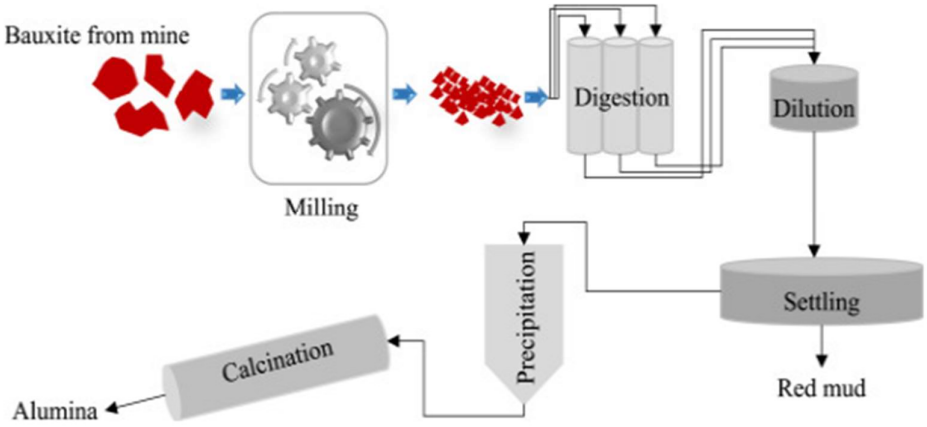

Figure 1: Bayer process flow diagram [15].

The second stage involves the electrolytic reduction of aluminum oxide to aluminum. The electrolytic process, known as the Hall-Héroult process, is carried out in smelting plants and is the most energy-intensive stage in the aluminum production chain requiring massive amounts of electricity [12]. The Hall-Héroult process is a fused salt electrolysis that comprises aluminum oxide's breakdown into aluminum and oxygen using direct current [12]. The electrolytic cells, shown in Figure 2, pass a direct current from carbon anodes through a molten bath of dissolved alumina and cryolite which deposits the denser

aluminum at the bottom of the cell where it is transferred to the casthouse [12]. All together it takes approximately 4 to 5 tonnes of bauxite ore to produce 2 tonnes of alumina. In turn, it takes approximately 2 tonnes of alumina to produce 1 tonne of aluminum [16].

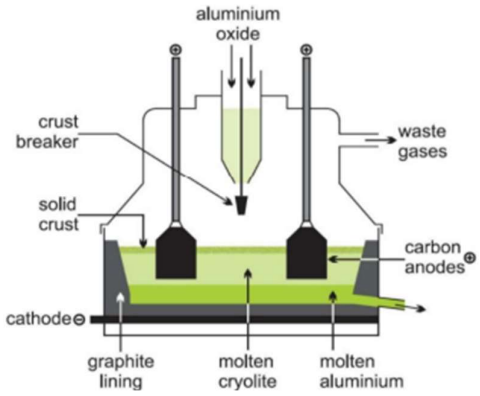

Figure 2: Electrolytic cell in aluminum production [12].

2.1.2 Alloys

A four-digit numerical system is used to identify wrought aluminum and aluminum alloys. In the 1xxx group, the aluminum content is the main consideration and other elements are considered only as impurities, which are either tightly controlled or have natural impurity limits [13, 17]. For the 2xxx through 7xxx series, first digit indicates the group or series it belongs to depending on its major alloying element. An exception is the 6xxx series alloys in which the proportions of magnesium and silicon available to form magnesium silicide are predominant [17]. A summary of typical alloys can be seen in Table 1.

Table 1: Typical aluminum alloys. Adopted from [13, 17].

Major alloy element	*Content in mass fractions (w/%)*	*Series*	*Product*	*Some typical uses*
Aluminum	≥99.00	1xxx	Sheet, Extrusions	Electrical conductors
Copper	Up to 4.5	2xxx	Sheet, Extrusions, Castings	High-strength aircraft parts
Manganese	1.25	3xxx	Sheet	Sheet-metal work, pots, pans, etc.
Silicon	Up to 13	4xxx	Castings	Motor parts, castings of all types
Magnesium	Up to 5	5xxx	Sheet	Marine uses, boats, fish boxes, can lids
Magnesium and Silicon	0.7 Mg 0.4 Si	6xxx	Sheet, Extrusions	Architectural extrusions
Zinc, Magnesium, and Copper	5.8 Zn 2.5 Mg 1.4 Cu	7xxx	Sheet, Extrusions	High-strength aircraft

In aluminum alloys other elements are intentionally added to improve the properties of the aluminum. Many alloys have been developed with the aim of improving the strength while retaining the desirable properties of aluminum such as its lightness and corrosion resistance [12]. Usually while the addition of an alloying element will increase the strength, it will reduce the resistance to corrosion, which makes it necessary to find a balance to achieve the properties which are necessary for the materials application [12]. A good example of the necessity of balance can be found with the AA7075 aluminum alloy which uses zinc, magnesium, and copper as its primary alloying elements. This alloy exceeds structural steel in strength [8], however the use of a small amount of copper as alloying element reduces corrosion resistance properties to some extent, as aluminum-copper alloys have very poor resistance to corrosion [12]. The 7075 alloy is an excellent choice for structural applications, but this slight reduction in corrosion resistance will limit its use in more corrosive environments, for instance near saltwater.

2.1.2.1 Temper

Aluminum alloys are classified as either heat-treatable or non-heat-treatable, depending on their strengthening mechanism [8]. Heat-treatable aluminum alloys develop their properties by solution heat treating and quenching, followed by either artificial or natural aging. The heat treatment involves holding the material at an elevated temperature and controlled cooling. They may also be cold worked to add additional strength or annealed for maximum ductility [18]. Heat-treatable alloys have copper, magnesium, or zinc as their primary alloying elements, and are found in the 2xxx, 6xxx, and 7xxx series of alloys. The wrought aluminum alloys that can only be strengthened by strain-hardening, otherwise known as cold working, are designated as non-heat-treatable [19]. These alloys are made stronger and harder through permanent deformation, and consist of the 1xxx, 3xxx, and 5xxx series alloys. Temper designations identifiers follow the series number of the aluminum alloy separated by a hyphen. Tempering refers to the alteration of the mechanical properties by means of either a mechanical or thermal treatment [19]. A list of the basic temper designations can be seen in Table 2.

Table 2: Basic temper designations per ANSI H35.1/H35.1(M)-2009 and adopted by the European EN 515 and ISO 2107 temper designation systems [20].

Identifier	*Description*
F	As fabricated and no mechanical properties specified (F stands alone)
O	Annealed to obtain lowest strength temper (O may be followed by a digit to indicate an annealed condition with special characteristics)
H	Strain-hardened wrought products with or without additional thermal treatment to reduce strength (H always is followed by two or more digits)
W	Solution heat-treated (W is an unstable temper due to natural aging at room temperature after solution heat-treatment)
T	Thermally heat-treated to produce stable tempers other than F, O, or H (T is always followed by one or more digits)

2.1.2.2 6xxx series alloys

The 6xxx series, also known as Al-Mg-Si alloys, are the focal material group of this thesis. These are very widely used aluminum wrought alloys due to their advantageous combination of cost and mechanical properties. 6xxx series aluminum have good strength and ductility, enhanced corrosion resistance, ease of formability, and good weldability which makes them strong candidates for structural applications [21]. The 6xxx series are referred to as a "soft" alloy which refers to their ease of extruding. They constitute the majority of extrusions produced and are used extensively in building, construction, and other structural applications [19]. Most of the 6xxx series Al alloys are used in T4 or T6 temper conditions. T4 indicates that the alloy is solution treated and is naturally aged to a stable state without the support of the cold work. T6 implies that the alloy is solution heat-treated, and without any cold work, it is artificially aged to achieve precipitation hardening [21].

The properties of 6xxx series alloys vary with composition and processing such as hot working, cold working, annealing, and aging processes [22]. The main alloying elements in this group are predominantly Si and Mg, which significantly affect the alloy properties [23]. Alloys in the 6xxx series contain silicon and magnesium approximately in the proportions required for the formation of magnesium silicate (Mg_2Si) precipitates, thus making them heat treatable [24]. The presence of higher Si content usually results in more formable alloys with higher strengths, which are susceptible to intergranular fracture and corrosion attack. Alloys with excessive Mg content exhibit low strength in artificial aged tempers with excellent corrosion resistance, and are considered more recyclable than excess Si alloys [23]. Table 3 shows common alloys and their percentages of Si and Mg. In their annealed state, the 6xxx series alloys offer a yield strength of 40-80 MPa and ultimate tensile strength (UTS) of 85-150 MPa. Significant increase in yield strength and UTS are exhibited after T6 treatment, with yield strength ranging from 210-360 MPa and UTS ranging from 240-385 MPa [22]. However, the ductility is reduced after T6 conditioning. T6 conditioned alloys demonstrate properties of 10-15% elongation as compared to 18-35% in the annealed state [22].

Table 3: Percentage of Si and Mg in common 6xxx alloys [24].

Alloy	*Si (%)*	*Mg (%)*
6005	0.60 - 0.90	0.40 – 0.60
6061	0.40 – 0.80	0.80 – 1.2
6063	0.20 – 0.60	0.45 – 0.90
6082	0.70 – 1.3	0.60 – 1.2
6106	0.30 – 0.60	0.40 – 0.80

2.2 Extrusion process

Extrusion is a process which converts a cast billet of solid metal into a continuous length of uniform cross-section by forcing it to flow through a die which is shaped to produce the required form of product. It is generally a hot working operation, with the metal being heated to give it a suitable degree of softness and ductility [25]. There are two methods of extrusion, referred to as direct and indirect, and they are classified depending on the arrangement of the tools in the process. In the case of direct extrusion, a die is located at one end of a container which a billet is loaded into. A ram pushes the billet, relative to the stationary container, through the die where the desired shape extrudes from the other side in the direction that the ram travels. For indirect extrusion the die is on the end of the ram, which is hollowed out to allow extruded material to pass through. An example of each tool arrangement can be seen in Figures 3 and 4. While direct extrusion is the more commonly used method, due to the more simplistic design and flexibility of achievable profiles, the arrangement of the tools and the fact that the billet moves within the container has negative consequences. The friction caused between the billet and the container increases the amount of work during the extrusion press cycle which results in an increase in temperature from the front to the rear of the extrusion that can produce changes in the metallurgic structure along the length of the extrusion [26]. The indirect extrusion process is free from the problems cause by friction, as the billet does not move within the container. This provides more consistency with dimensions, grain structure, and mechanical properties. Though, in this tool arrangement the extrusion must travel through an opening in the ram resulting in a reduced achievable profile size [26].

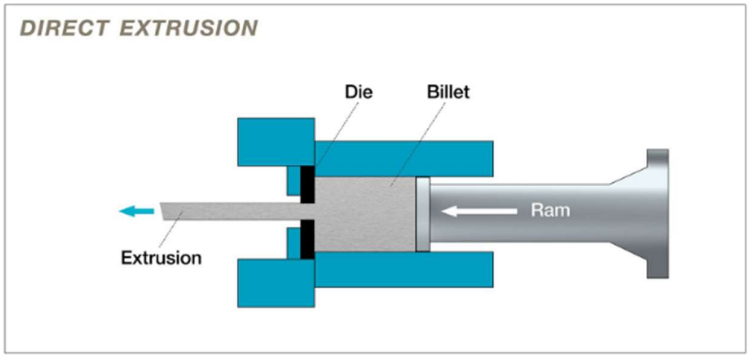

Figure 3: Direct extrusion illustration [26].

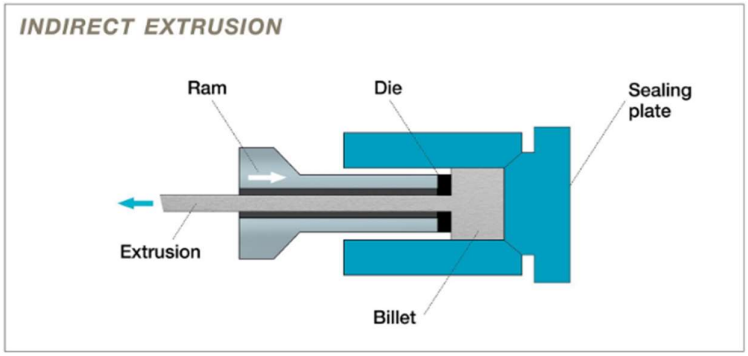

Figure 4: Indirect extrusion illustration [26].

Extruded shapes are categorized as either solid or hollow. In the case of hollow extrusions there can be one or multiple voids within. For multiple void extrusions, the cross-sectional area is bordered by a single continuous curve defining the outer perimeter and an internal curve for each enclosed void [27]. For hollow extrusions, the most commonly used method is the welding chamber concept in which the stream of flowing metal is first divided into distinct streams and subsequently rejoined by a pressure weld [25]. This method uses an upper and lower die to separate the billet into channels which are called portholes. An example of this die setup can be seen in Figure 5. The mandrel is used to form the inner contour of the profile, the welding chamber accumulates and welds the material it into an integral body, and the metal flows out between the tip of the mandrel and the die aperture to form a tube or hollow section depending on the shape selected [25, 28].

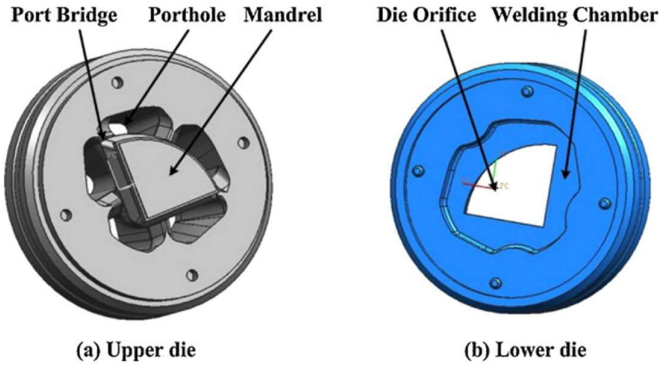

Figure 5: Upper and lower hollow extrusion die [28].

After extruding, the still hot aluminum profiles need to be cooled. This is typically done by introducing the extruded aluminum profiles to a water bath to cool them quickly and uniformly in a process called quenching. This is an important step in the extrusion process because the rapid cooling is necessary to retain the alloying elements and safeguard the required mechanical properties and microstructure of the metal. However, cooling too rapidly can cause severe thermal stresses which may lead to severe distortion [29], which can negatively affect downstream processes. This leads to a balance of operation between cooling as rapidly as possible to achieve maximum strength, and cooling as slowly as possible to avoid residual stresses and distortion [29]. Some extruded products are mechanically stretched, to alleviate natural as well as quench induced internal stresses, which alleviates some pressure on cooling the profiles more quickly.

2.2.1 Extruded profile tolerances

For profiles which are brought to their final dimensions by extruding, the European Committee of Standardization has published the standard EN 755-9 for tolerances on dimensions and for general applications and EN 12020-2 for precision profiles in alloys AW-6060 and AW-6063. EN 755-9, which is used in this thesis, specifies the tolerances on dimensions and form for aluminum and aluminum alloy extruded profile with a cross section contained within a circumscribing circle not greater than 800 mm [30]. This addresses tolerances on cross-sectional dimensions, as seen in Figure 6, as well as length and squareness on cut ends. Tolerances on forms are including straightness, convexity-concavity, contour, twist, and angularity.

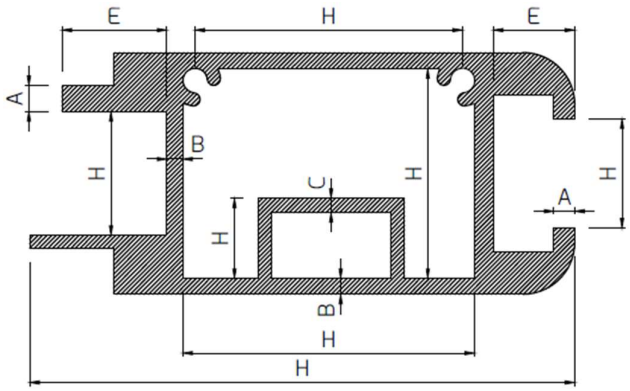

Dimension	Definition
A	Wall thickness except those enclosing the hollow spaces in the below profiles.
B	Wall thickness enclosing the hollow spaces in hollow profiles except those between two spaces hollow spaces.
C	Wall thickness between two hollow spaces in hollow profiles.
E	The length of the shorter leg of profiles with open ends.
H	All dimensions except wall thickness

Figure 6: Definition of cross-sectional dimensions in EN 755-9 [30].

The tolerances for the outer dimensions, inner dimensions, and wall thicknesses of a hollow profile are dependent on the overall cross-sectional size, or circumscribing circle diameter (CD) with which the cross-section will fit into. As this CD becomes larger, the achievable tolerances become larger as well. Similarly, as the individual dimensions themselves become larger their tolerances become larger, and this compounds when the CD of the overall cross-section grows. An example regarding dimensions falling within the category H, from Figure 6 above, can be seen within Table 4. This type of tolerancing will be typical for any individual features within a hollow extrusion, however the individual features will also affect each other in some cases. An example of this is when a hollow profile has an open end. For this type of profile, the tolerances for the leg of the opening, E, will need to be added to the tolerance of the overall height of the of the opening, H, to get the new achievable tolerance for H. The location of the feature can also have an effect on its tolerance. Wall thickness tolerances become higher as they move internally. For instance, wall thickness tolerance for an internally located dimension C will be higher than that of a wall thickness dimension A or B. In regard to profiles provided at fixed length, the tolerances on length are dependent on the CD as well as the length itself. As the profiles become bigger and longer, the tolerances will become larger as well.

Table 4: Tolerances on cross-sectional dimension H [30].

Dimension H (mm)		**Tolerances on H for CD size (mm)**		
Over	Up to & including	CD<100	100<CD≤200	200<CD≤300
-	10	±0.25	±0.30	±0.35
10	25	±0.30	±0.40	±0.50
25	50	±0.50	±0.60	±0.80
50	100	±0.70	±0.90	±1.10
100	150	-	±1.10	±1.30
150	200	-	±1.30	±1.50

Deviation from straightness, according to EN 755-9, is measured with the profile placed on a horizontal base plate so that its own mass decreases the deviation. The straightness is measured from the difference, over a specified length, of which the profile deviates from the straight base plate. The deviation from straightness shall not exceed 1.5 mm/m length and local deviations shall not exceed 0.6 mm/m length [30]. Similarly, twist is measured by placing the profile on a flat base plate resting under its own mass, but in this instance the measurement is taken as the maximum distance at any point along the length between the bottom surface of the profile and the base plate surface. Twist tolerance increases with the width and length of the profile. The tolerances for convexity and concavity, for hollow extrusions, is dependent on the width of the profile and the wall thickness. An example of how this is measured can be seen in Figure 7. Angularity is the measure of deviation from a specified angle. In the case of a right angle, the tolerance is dependent on the width of the part. As it becomes wider the tolerance is larger. The maximum allowable deviation in an angle other than right shall be ±1° and in case of unequal side lengths the tolerance on angularity shall apply to the shorter side of the angle [30].

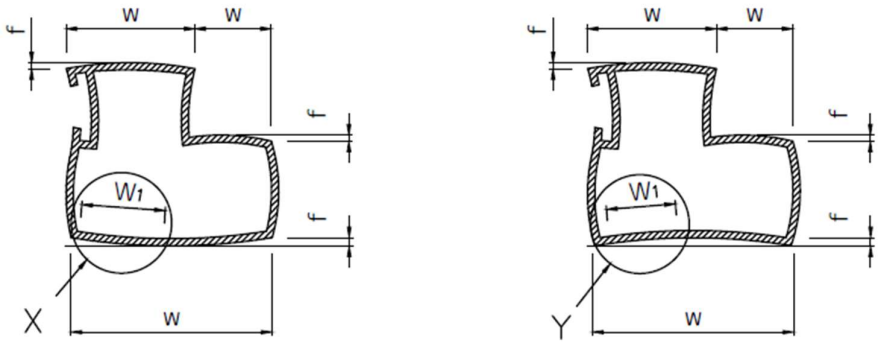

Width W (mm)		Deviation F (mm)	
Over	Up to & including	Wall Thickness t≤5 (mm)	Wall Thickness t≥5 (mm)
-	30	0.30	0.20
30	60	0.40	0.30
60	100	0.60	0.40
100	150	0.90	0.60
150	200	1.20	0.80

Figure 7: Convexity-concavity of hollow profile from EN 755-9 [30].

2.2.2 Factors affecting dimension and form accuracy in extrusion process

Extrusion defects may arise in extruded products from the starting material or billet, the deformation process itself, or from other post-processing corrective measures [31]. The chemistry of the billet should be optimized in accordance with the needs and expectations of the extruder [32]. The homogenization process for a cast billet is also an integral part of a successful extrusion process. When properly homogenized, a billet will give high throughput rates, low breakout pressures, desired shape within dimensional tolerances, uniform surface finish free from streaking and die-lines, as well as high tensile properties [32]. High extrusion temperatures lead to an increase in ductility of the alloy to reduce the force required for extrusion, whereas low extrusion temperature helps to achieve good geometrical tolerances [33]. Therefore, a balance must be struck to obtain an optimum heating temperature to achieve sound geometrical tolerances while simultaneously reducing force.

The extrusion speed is highly dependent on the extrudability of an aluminum alloy, based on the effects of its alloying elements. For example, the extrusion speed applicable to AA7075 (1-2m/min) is only a small fraction of that for a medium-strength 6xxx series alloy such as AA6061 (5-25 m/min) [34]. The speed of the ram during the profile extrusion process is a critical parameter which affects the resulting surface quality, mechanical behavior, metal flow uniformity, and heat effect. With too high of ram speed, large nonuniformity of metal flow in extrusion process occurs, which often leads to defects such as twist deformation, cracking, or surface burning of the extrudates [28]. With decreasing extrusion speed will come increased extrusion load and prolonged contact time between tools and the hot billet. As the die wears, there will be an effect on the extruded products dimensional tolerance. Too high of an extrusion load will lead to an intolerable amount of wear in a die, which is the major cause of die failure [34]. The die is perhaps the most vital component in extrusion because of its high cost, very fine dimensional tolerances, and good performance against repeated thermo-mechanical stresses [35]. As ram speed is found to have a very high influence on both extrusion load and dimensional accuracy [33, 34], it is critical to optimize ram speed to achieve high productivity, economical tool life, and dimensional accuracy.

Extruded profiles with complex shapes, hollow sections, and varying thicknesses can have the inability to cool uniformly during the quenching process. This non-uniform cooling, both across the section and along the length of the section, may lead to large temperature gradients and cause high residual stresses and thermally induced distortions, such as warping and twisting [36]. For semi-finished product forms, the reduction in these residual stresses revolves around the application of plastic deformation by stretching or cold compression. For complex geometries, it is more difficult to plastically deform the product so the thermal gradients must be managed by using less aggressive quenching regimes [37]. After stretching to the desired straightness, the profiles are typically cut to the length requested by the customer.

2.3 Langenuen suspension bridge

The Langenuen suspension bridge is a proposed infrastructure project in Norway, as part of a larger E39 Costal Highway Route in western Norway, aimed to replace ferries with bridges. Aluminum is being investigated as an alternative girder material for this project. Spanning 1,720 meters over the Langenuen Fjord with 1,250 meters of which would be aluminum, this would be the longest aluminum bridge in the world [38]. An illustration of the proposed design can be seen in Figure 8.

Figure 8: Illustration of proposed Langenuen suspension bridge [39].

Three competing aluminum girder concepts are developed for the Langenuen suspension bridge. The first of which is discussed is the panel concept shown in Figure 9. This concept utilized the possibilities of extruded aluminum profiles in combination with FSW. By using panels made from hollow profiles, a very stiff structure with little need for supporting structure is created, which reduces weight and assembly time [39]. The dimensions of this bridge girder is 34 m in width, 5.5 m in heigh, and built in 12 m long sections. Each section is to have a bulkhead where cables are connected via hangers. The top deck panels are built up from 150 mm high extrusions that are FSW together. Side and bottom panels are built similarly, but with 115 mm thick FSW panels. The bottom panels are integrated with three T-beams to give sufficient buckling resistance in the lower part of the bridge. The alloy that is intended to be used for all profiles is EN AW6005A-T6, with an alternative for EN AW6082-T6 [39].

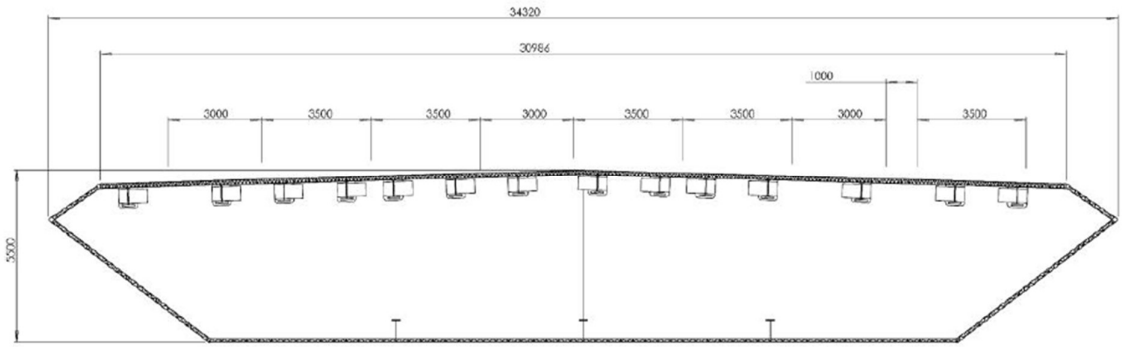

Figure 9: Cross-section of panel concept [39].

The second concept to be discussed is the plate concept, Figure 10, which is based on a more standardized bridge girder cross-section design. The panel concept is 32 m in width and 5.5 m in height. The bridge deck is supported every 4 m with bulkheads and hangers every 12 m. The cross-section skin consists of stiffened plates with a thickness of 28mm and stiffeners located at a maximum center distance of 1 m, with the stiffeners being located closer together below the road deck [39]. This design has a T-beam going around the entire cross-section, and four sets of trusses to transfer local forces to the edges.

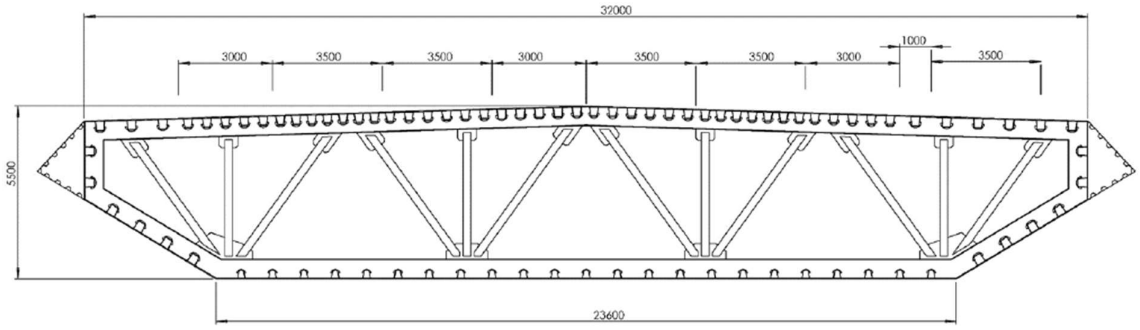

Figure 10: Cross-section of plate concept [39].

The third and final design is referred to as the transverse panel concept. This girder concept consists of extruded panels in all parts of the outer skin. This girder is 35.4 m in width and 5.5 m in height with. The deck is supported by transverse bulkheads every 3.9 m and hangers every 11.7 m. An example of the girder cross-section and top and bottom panel detail can be seen in Figure 11. In this figure only half of the girder is showing which is intended to display internal detail and symmetry. In this design the panels are running

transversely to avoid the discontinuity of welds created by limited access to welds created by running panels longitudinally. The connection of the decks to the bulkhead is managed by a separate joiner profile.

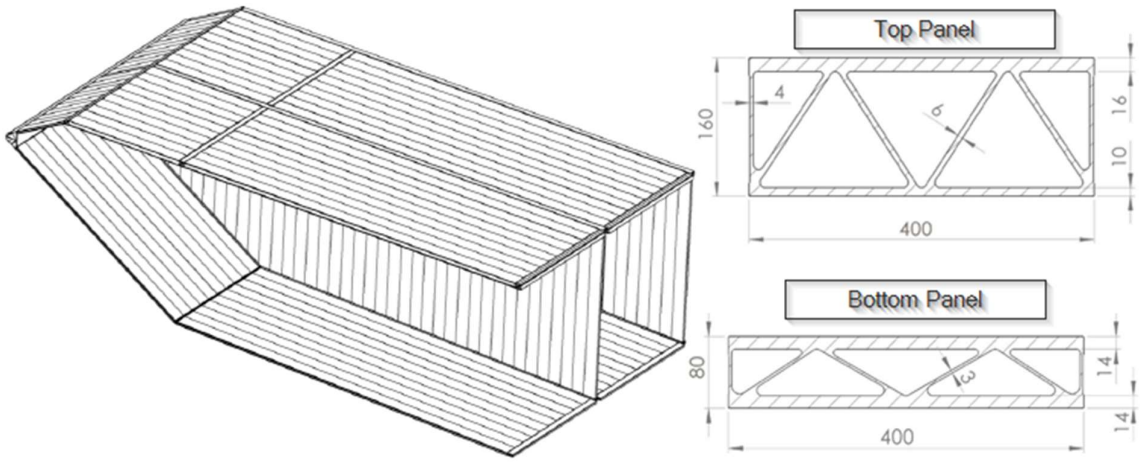

Figure 11: Transverse panel concept with top and bottom panels [39].

2.4 Friction stir welding

Friction Stir Welding is a solid-state joining process which was invented in 1991 at The Welding Institute in Cambridge, England. This process involves the use of a non-consumable, rotating tool which is plunged with a downward force into the work piece, and traverses along the weld seam to plastically deform and mechanically intermix the two materials [40]. Unlike traditional fusion welding techniques, FSW does not bring the materials being joined to their melting points and typically has no need for filler material or shielding gases. The fact that the materials are not brought to their melting points is a major advantage of this technology, as it eliminates most of the negative effects associated with the cooling and resolidification which are inherent to conventional fusion welding [41]. FSW has also been able to join most types of aluminum alloys, even those which are classified as non-weldable by fusion welding due to hot cracking and poor solidification microstructure in the fusion zone [42].

During the FSW process, the rotating tool is plunged into the two abutting plates which are being joined until the shoulder makes contact with the plates. The probe, or pin, is penetrating to near full depth of the thickness between the plates. The tool continues to rotate while moving along the seam to be joined, and the softened material is literally stirred together forming a weld without melting [42]. At the end of the weld the tool is retracted while continuing to rotate, leaving a hole at the end of the weld. The side of the weld for which the rotating tool moves in the same direction as the traversing direction is commonly known as the advancing side (AS), while the other side where the tool rotation opposes the traversing direction as known as the retreating side (RS) [43]. A schematic which illustrates this is shown in Figure 12. FSW involves complex material movement and plastic deformation with the welding parameters, tool geometry, and joint design exerting significant effect on the material flow pattern and temperature distribution, thereby influencing the microstructural evolution of the material [42]. The main process

parameters used to control the FSW process are downward force, tilt angle, rotation speed and welding speed. The effect of each parameter can be seen in Table 5.

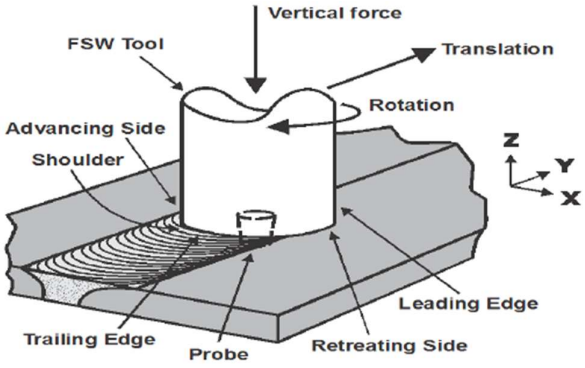

Figure 12: Schematic illustrating FSW process [43].

Table 5: Main process parameters in FSW [42].

Parameter	Effects
Rotation speed	Frictional heat, "stirring", oxide layer breaking and mixing of material.
Tilting angle	The appearance of the weld, thinning.
Welding speed	Appearance, heat control
Downward force	Frictional heat, maintaining contact conditions.

FSW can be used to produce butt, corner, lap T, spot, fillet and hem joints, weld stock with different thicknesses, tapered sections, as well as to weld hollow objects such as tanks, tubes, and pipes [44]. The design of the fixture plays an important role in the FSW process as there are large forces at work. The fixture should be designed and fabricated in such a way that it is able to bear the high magnitude of forces and high temperature during the welding process [43]. The base metal to be welded are rigidly held with the help of specially designed clamps which are designed in such a way that they do not protrude after being mounted on the anvil to avoid obstruction of the welding tool [45]. An example of a fixture and its components can be seen in Figure 13. The fixture is responsible for restraining the plates from all directions to avoid dragging, opening, or lifting of the plates during welding.

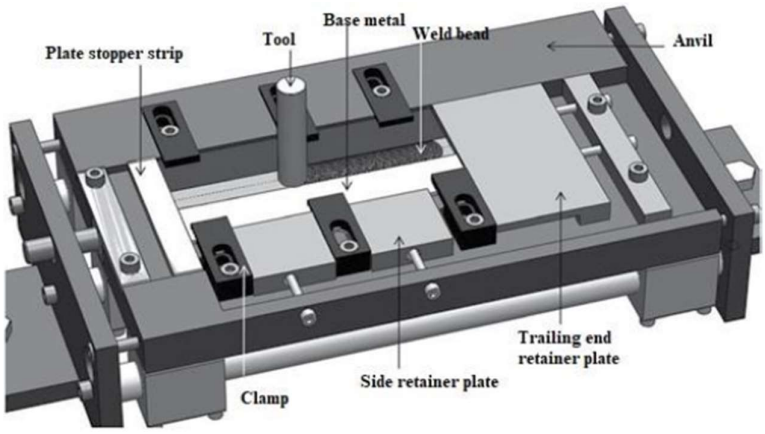

Figure 13: Example of FSW fixture [45].

2.4.1 Capabilities and characteristics of FSW

FSW can process a variety of thickness of aluminum, generally ranging from 0.5 mm to 65 mm when being welded from one side at full penetration, without experiencing porosity or internal voids [46]. To assure high repeatability and quality the equipment must possess certain features. A conventional CNC can be used for most simple welds, but as the material thickness increases, purpose-built FSW equipment becomes essential [47]. With proper machinery, welding speeds in FSW can exceed those in conventional joining processes for aluminum. A typical FSW speed for 5 mm thick AA6082 is stated between 250 mm/min and 400 mm/min using a CNC machine which is not designed for the high speeds or high down forces needed in FSW. With production machines, speeds of 2000 mm/min are achievable using the same alloy and thickness [46].

2.4.2 FSW zone structure

FSW involves complex interactions between simultaneous thermomechanical processes which affect the heating and cooling rates, plastic deformation and flow, dynamic recrystallization phenomena, and the mechanical integrity of the joint [48]. This results in different microstructural regions of the resulting weld, as seen in Figure 14. The nugget zone (NZ) is where the intermixing of the material is taking place, where the thermo-mechanically affected zone (TMAZ) is the zone of maximum deformation without intermixing, and the heat affected zone (HAZ) experiences the temperature variation without any deformation [49]. The NZ, also referred to as the stir zone, is a region of deeply deformed material that corresponds approximately to the location of the probe during welding [48]. The size of this region is dependent upon the diameter of the tool pin and this zone experiences grain refinement due to the dynamic recrystallization [45]. The TMAZ represents the entire deformed zone underneath of the tool shoulder other than that which is in the NZ. Material within this zone experiences thermal cycles as well as mechanical deformation due to the spinning motion of the tool shoulder. The thermal effects on this region are comparatively less than in the NZ which shows a lower degree of deformation and partial recrystallization of grains [45]. The HAZ is common to all welding processes. In FSW this zone represents the area which is not mechanically deformed but is affected by the thermal cycles created during the joining process. When this region is subjected to temperatures more than the recrystallization temperature of the material, grains are coarsened and the density of the strengthening agents in the alloy is reduced causing it to become the low strength region in the welded joint [45]. When the region experiences lesser temperatures than the recrystallization temperature during the process, then the low strength region of the weld shifts from the HAZ to the TMAZ [45].

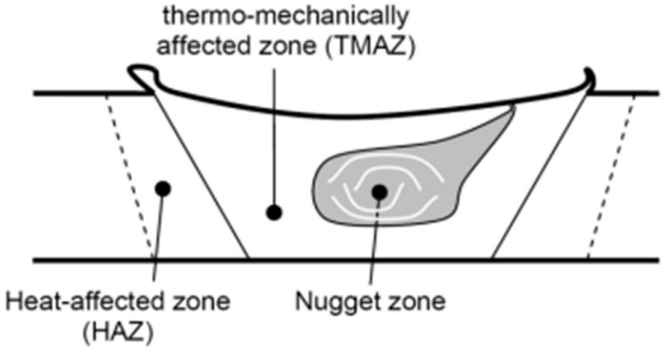

Figure 14: FSW cross-section [48].

2.4.3 Common defects in FSW

Low heat generation is one of the most prominent causes of defect formation in FSW as the heat produced softens the material directly under the shoulder, however this does not mean that excessive heat input can improve the joint quality [50]. At lower heat input, insufficient softening of the welded material occurs, and flow stresses increase which leads to inefficient consolidation and inadequate mixing. If the heat input is too high the resulting grain growth can cause the joint to become hard and brittle, reducing the strength and ductility of the joint [50]. Table 6 shows some of the most common defects which occur in FSW, along with their causes.

Table 6: Common defects in FSW, locations, and causes [50].

Defect	Location	Cause
Tunneling	On AS between the TMAZ and the stir zone under the surface of the weld	1) Low plunge depth; 2) Too high welding speed; 3) Inappropriate pin offset; 4) Too low rotational speed;5) Improper tool geometry
Kissing bond	At interface in stir zone	1) Improper removal of oxide layer from faying surface;2) High welding speed;3) Inadequate material movement
Void	On AS of the weld, on or beneath the weld surface	1) Too high welding speed; 2) Improper forging pressure; 3) Improper tool tilt
Joint line remnant	At the root of the weld or in the stir zone in the remnant of original faying surface	1) Inadequate removal of oxide; later from pate edges; 2) Poor tool-to-joint alignment
Incomplete root penetration	Below the stir zone at the interface of the faying surface	1) Local variations in the plate thickness; 2) Improper tool design; 3) Inappropriate plunge depth; 4) Too short pin length
Hooking	TMAZ of AS and RS in lap welding	1) Low welding speed; 2) High rotational speed; 3) Improper tool design; 4) Inadequate tool tilt

2.5 FSW gap tolerance related literature

The FSW process can handle some small gaps and misalignments, caused by variation in part fit-up, without severely affecting the joint quality. A gap is defined as the perpendicular distance, or planar displacement, between the faying surfaces of the weld joint. This is most often caused by lack of straightness in the parts and, depending on the exact condition and amount of gap, it may or may not be able to be removed with fixture clamping [51]. If the clamping forces cannot remedy the gap condition, and the parts are too costly to reject and cannot be improved through additional manufacturing processes, the gap condition must be managed effectively. As mentioned previously, the welding

temperature and material flow around the pin will have a significant effect on the resulting joint quality. If the gap becomes too large for the process to handle, the gap can cause material missing and frees the constraint force at the gap site in front of the tool, thereby affecting heat generation and material filling in the weld [52]. The lack of heat generation is caused by the decrease in frictional area between the tool surfaces and the abutting plates in the area of the gap. This reduces the efficiency of the frictional heat generation between the tool and the plates, and this reduction becomes more severe as the diameter of the gap grows larger [52]. In regard to material flow, studies currently suggest the shear layer around the pin is primarily responsible for this transfer [52]. Because of the effect of the plunge depth and tilt angle of the tool, the height of the leading shear layer must be taller than that of the trailing one. In a gap-free condition, the material in the leading shear layer would be partially transferred to the trailing shear layer to form the weld. However, when the faces of the plates are not in close contact, the leading shear layer volume would be decreased because of insufficient material inflow [52].

The permissible gap, without significantly lowering the UTS, varies in the papers reviewed, but generally falls between 10-20% of the base material's thickness. Ma et al. conducted an FSW experiment using 6.2 mm thick 2A12-T6 alloy at gaps of 0.8, 1.6, and 2 mm [52]. The joint efficiencies were found to be 73% with a gapless weld, 71% with 0.8 mm gap, 68% with 1.6 mm gap, and dropping significantly to 43% at the 2 mm gap. The study concluded that only 0.8 mm, or 13% of the materials thickness, gap tolerance should be permitted. It was found that kiss bonding and voids occurred at 1.6 mm gap and at 2 mm gap the tunnel defect occurred. Tsarkov et al. performed a similar experiment, this time with 5 mm thick AA5083 alloy at gap widths of 0.5, 1.0, 1.5, and 2 mm [10]. The cross-sections of the welds over the gaps of up to 1.5 mm showed clean and smooth welds. The UTS outcomes were not discussed in detail, but the study concluded that the FSW process was tolerant enough to alloy gaps of up to 20% plate thickness, although it inevitably leads to a reduction in local section thickness if no filler material is added. Widener et al. investigated FSW with 3.2 mm 7075-T73 across a wedged gap [53]. The plates were gapless at one end an increased to a 1 mm gap across a total distance of 686 mm. The study concluded that there were only minor variations in the tensile properties along the weld joint. At a gap width of 0.81 mm, or 25% of the material thickness, volumetric defects were found in the weld nugget. Additionally, the study states that though there was thinning of the weld nugget as the gap increased, however because the nugget material is stronger than the HAZ, the thinning in the nugget does not adversely affect overall tensile strength.

In a study performed by Cole et al., a 25-run fractional factorial DOE was performed to investigate the effects that spindle speed, travel speed, travel angle, gap width, mismatch, and tool misalignment would have on the mechanical properties of a FSW produced weld on 5 mm thick 5083-H111 alloy [51]. The experiment was an orthogonal design for the six process factors to be tested at five levels, with three tensile samples taken from each weld. Nominal welding and set up parameters were established, and the process stability to was tested before the experiment. The study found that UTS, yield strength, and elongation begin to decrease when either tool offset distance from weld centerline or gap in abutted plates exceeds 25% of the average pin diameter (6mm). This correlates to the process tolerating gaps of up to 1.5 mm, or 30% of the thickness of the material being joined. However, as the length of weld along the gap increases the material stored beneath the tool diminishes, providing less material to fill the mating void . The process was also found to tolerate a 2.5% vertical mismatch and 10% plate thickness variation. In terms of welding parameters, it was interpreted that spindle speed and travel speed had the least

significant effect on the mechanical properties of the weld and are least effective in managing production variations. Travel angle on the other hand showed higher significance in relation to UTS and elongation response and has the highest potential of all parameters to manage or correct for productions variations.

Shultz et al. had similar finding pertaining to the usefulness of higher travel angle toward mitigating the effects of welding in the presence of a gap [54]. They experimented with welding 5 mm thick 5083-H111 with gaps of 0.0 to 2.0 mm, at 0.5 mm increments, and travel angles of 1 deg, 3 deg, and 5 deg. When welding gaps in excess of 1.0 mm, a travel angle of 5 deg was able to produce higher joint efficiencies that those made at 1 deg and 3 deg. At 5 deg, a joint efficiency of 85-90% is maintained from zero-gap to 1.5 mm, whereas those of 1 deg and 3 deg decrease to values below 70% at and above the 1 mm gap width.

Singh et al. performed an experiment to see what effects the shape of the pin has on FSW over a controlled gap width [55]. This study was performed using 6mm thick AA6082-T6 with a controlled gap width of 1.2 mm, or 20% of the materials thickness. The three types of pin profiles investigated are a plain cylindrical taper tool, cylindrical threaded taper tool, and straight cylindrical threaded tool. Both of the tapered pins produced welds with defects in the presence of the gap. The plain cylindrical tool pin was unable to produce sufficient heat to plasticize the material completely due to low availability of material in confinement of the tool pin. This resulted in unbounded regions and tunnel defects throughout the welds. The cylindrical threaded tool pin generates higher heat in the NZ under the same conditions as the plain cylindrical pin but is unable to consolidate plasticized material under the tool shoulder. The tool shoulder loses control over the plasticized material which results in surface defects as well as unbounded regions and tunnel defects. The straight cylindrical threaded tool pin was able to produce defect free joints in the presence of the gap. It is concluded that because the surface area of the straight cylindrical pin is larger, it has more contact with the material at the interface. This raises frictional heat to an appropriate level to create local softening and improve the flow of material to mitigate the gap effect.

To aid in compensating for large gaps, additional material can be added to counteract the thinning of the weld, volumetric defects, and loss of strength. Vertical compensation friction stir welding (VCFSW) is a technique which adds a compensation strip of material at the interface of the two workpieces to be welded. A study by Ji et al. investigates the use of VCFSW to weld 4mm thick 6061-T6 alloy with gaps of 1.0 and 1.5 mm [56]. The compensating strip used is 2024-T4 alloy. The article states that the compensation strip is of a different alloy because if it was the same as the base material the frictional heat is typically not enough to break up the compensation strip and mix it adequately with the base material. In order to successfully get high-quality joints and realize the joining process, a compensation material with a lower melting temperature should be chosen. Before testing with the compensation strip, the authors tested the process in the presence of a 1.0 mm gap, or 25% of the thickness of the base material, without the compensation strip and confirmed that the process was not successful and resulted in groove defects in the weld zone. The process was able to produce defect free welds at 1.0 mm gap with the 2024-T4 compensation strip, but not at 1.5 mm. At 1.5 mm gap, the amount of 6061-T6 alloy within the weld zone decreases and the amount of 2024-T4 increases. Because the melting point of 6061-T6 is higher, and the frictional heat acting upon it is much larger, the frictional heat within the weld zone, with larger amounts of 2024-T6 present, is decreased beyond adequate conditions. Also, the 2024-T6 alloy owns higher hardness and strength at elevated temperatures than the 6061-T6 alloy, leading to higher flow stress.

At 1.0 mm gap width, compensating with the 2024-T4 alloy was able to create a maximum joint efficiency of 71.5% of the base material. This was achieved at the lowest weld speed tested, 50 mm/min, and the UTS descended as the welding speed increased.

A study by Abu-Okail et al. similarly experimented with filling a gap with a compensating strip of a different alloy [57]. This experiment used 3.5 mm thick base material of AA2024 alloy and compensated with AA7075 strips to fill the gaps from 1.0 to 3.0 mm at 0.5 mm increments. Again, the compensating material used has a slightly lower melting point and higher UTS when compared to the base material. At 1.5 mm, the weld was found to have the most desirable characteristics, achieving UTS of 62.06% of the base material. Tsarkov et al. also experimented with adding filler material to compensate for a gap, choosing instead to used aluminum powder and plasticized wire of the same AA5083 alloy [10]. The powder was found to blow out of the gap when welding, producing low quality welds. Adding the additional wire into the gap, by use of a roller fixture, was concluded to produce sound welds with tensile strengths in the range of the base material. A list of the literature discussed within this section can be seen in Table 7.

Table 7: Related literature on FSW process with gaps

Author	Title	Year	Comments
Cole, E.G. et al.	Stability of the FSW process in presence of workpiece mating variations.	2012	Explores common process variations encountered in FSW and the limits to which acceptable joint strength is maintained while welding.
Ma, H., et al.	Gap-tolerance control for friction stir butt welding of 2A14 aluminium alloy	2019	Report the effects of gap variation upon the joint quality and thermomechanical behaviour of 2A14-T6 aluminium alloy friction stir butt welding.
Widener, C. et al.	Effect of fit-up tolerances on the strength of friction stir welds	2006	Investigate FSW with plate gap, determine if defects created by localized fit-up variations remain localized.
Shultz, E.F. et al.	Effect of Compliance and Travel Angle on Friction Stir Welding With Gaps	2010	Investigation of the effects of friction stir weld tool travel angle and machine compliance on joint efficiency
Singh, A., et al.	Influence of tool pin profiles on friction stir welding with a gap for AA6082-T6 aluminium alloy	2019	Influence of tool pin profiles and rotational speeds on friction stir welding joints are studied by the formation of a gap between the abutting plates.
Ji, S., et al.	Vertical Compensation Friction Stir Welding of 6061-T6 Aluminum Alloy	2016	Apply vertical compensation friction stir welding towards 4mm wall thickness 6061-T6 alloy.
Abu-Okail, M., et al	Production of tailor-welded blanks by vertical compensation friction stir welding technique	2018	Testing of varying vertical compensating strip widths in FSW process.
Tsarkov, A., et al.	The influence of gaps on friction stir welded AA5083 plates	2019	Investigation of butt-welded of 5 mm thick sheet 5083 aluminum alloy in the presence of joint gaps.

3 Experimental

3.1 Material

3.1.1 Chemical composition

Aluminum alloy 6082 with a T6 temper was used in this experimental work. The chemical composition of this particular alloy can be seen in Table 8.

Table 8: Chemical composition of AA6082 used in experiment

Alloying element (wt%)										
Si	Fe	Cu	Mn	Mg	Cr	Ni	Zn	Ti	Pb	Al
0.95	0.19	0.03	0.49	0.61	<0.01	<0.01	0.01	0.01	<0.01	Bal.

3.1.2 Extrusion

The material was cast, homogenized, and extruded using industrial standards at Hydro in Finspång, Sweden. A cross-section of the resulting extruded profile, a scaled down bridge deck profile for research purposes, which was used in this study can be seen in Figure 15.

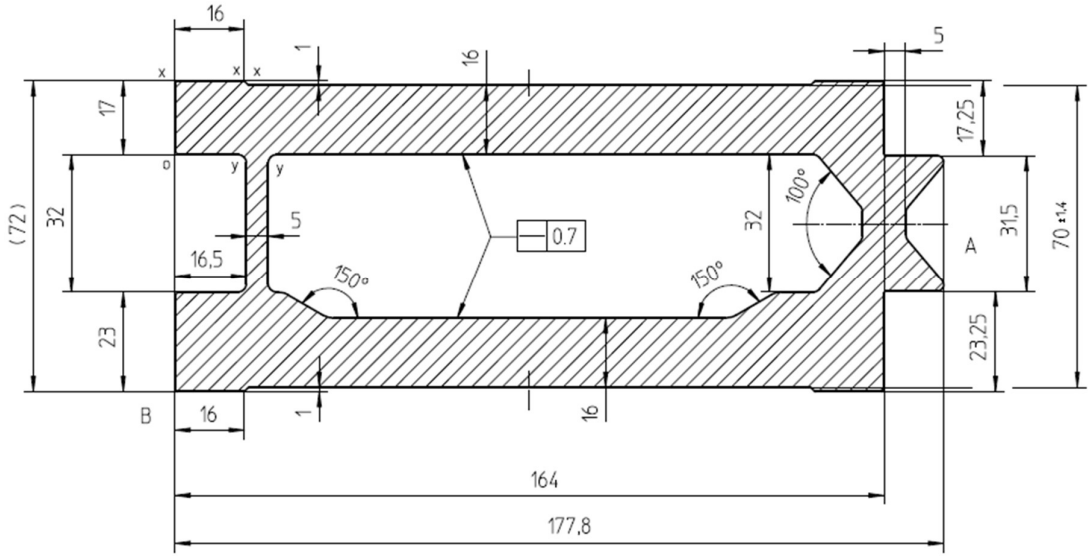

Figure 15: Cross-sectional view and dimensions of resulting extruded profile

3.2 Welding

The friction stir welding was performed with an MTS I-STIR™ PDS FSW machine at Hydro Innovation and Technology in Finspång, Sweden. The parameters and procedures which

were used during this experimentation were generated from the company's internal knowledge of the FSW process and further refined with multiple trial runs on gapless joints prior to the start of this thesis. All welds were performed with a 1.5 ° tool tilt angle, threaded tapered pin, and identical weld parameters. Due to confidentiality, the specifics of the FSW process parameters and tools used will not be discussed in detail within this thesis. The welding parameters were kept constant to isolate and analyze only the effect of the gap on the quality of the resulting welds.

In preparation for welding, the extruded profiles were cut to 1-meter lengths and deburred with a deburring tool to remove sharp edges and prevent fit-up issues caused by excess material. They were then blown off with high pressure air and wiped with a paper cloth to remove any remaining cutting chips and excess cutting fluids, and finally wiped with Ethanol (CH_3CH_2OH) and marked with an identifying number.

3.2.1 Fixture

The weld fixture used for experimentation was comprised of two side retaining rails, a stopping plate, and four vertical clamps, as can be seen in Figure 16. These fixture components were each made from mild steel. The first side retaining rail which was installed served as a guide for straightness along the direction of travel. A probe was used along this rail to align it with the travel of the machine tool within ±0.05mm over 1-meter of travel distance, before bolting it to the FSW table. The second side rail was bolted to the table and used a series of 10 bolts to apply lateral pressure to the profiles, preventing the profiles from separating from one another during welding, as well as providing the ability to make some adjustments regarding the consistency of the created gaps within the weld seam. The four vertical clamps were bolted to the table, and they were each torqued to 40 Nm, once the profiles were fitted in.

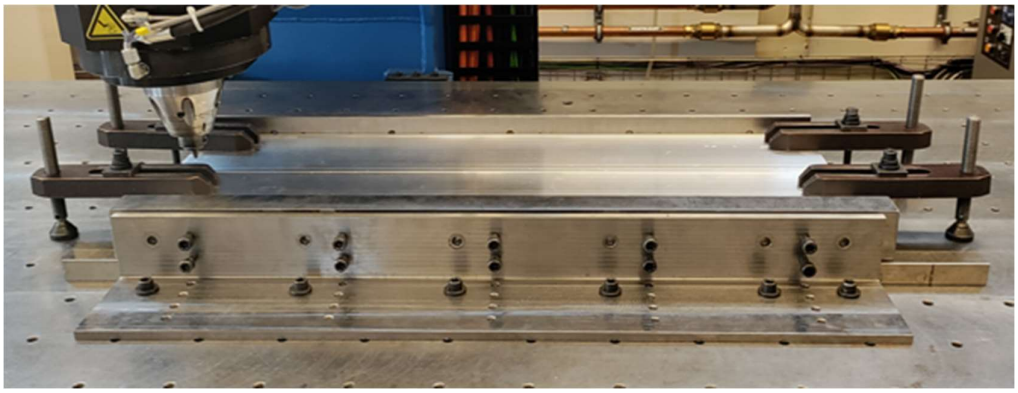

Figure 16: Fixture setup for welding 1-meter length profiles

3.2.2 Creating gaps and welding

The joining of two profiles within the fixture results in a 1-meter-long butt-joint on either side of the workpiece. The top butt-joint at 17 mm wall thickness and the bottom joint at 23 mm wall thickness. A gapless weld was performed on the 17 mm side of the workpiece, as can be seen in Figure 17. Following this, gaps of 1.0, 1.5, 2.0, and 3.0 mm were created between the two profiles using steel spacers on each end of the joined profiles. First the spacer was placed against the bottom, 23 mm thickness side of the profile, and then the second profile was inserted, and the spacer was placed into the top, 17 mm thickness side

before the profiles were pressed together. An example of this can be seen in Figure 18. Spacers were not used in the center because the spacers would then have been required to be made from aluminum and would be consumed within the weld. This would not have represented a realistic scenario during production, and would add material into the welded gaps, influencing the results.

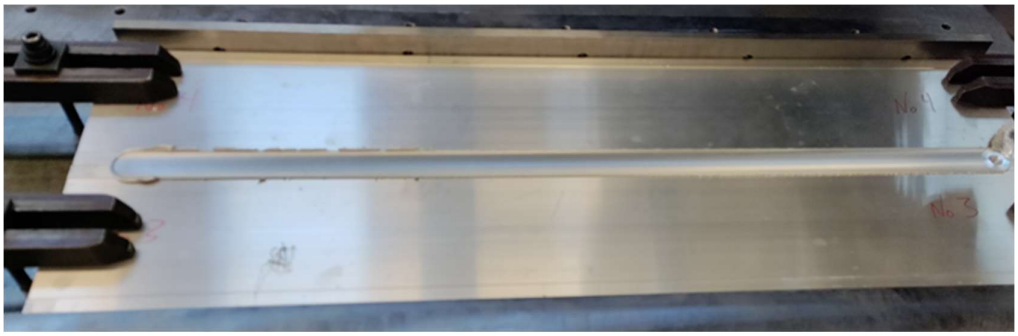

Figure 17: Gapless weld of 17 mm thickness

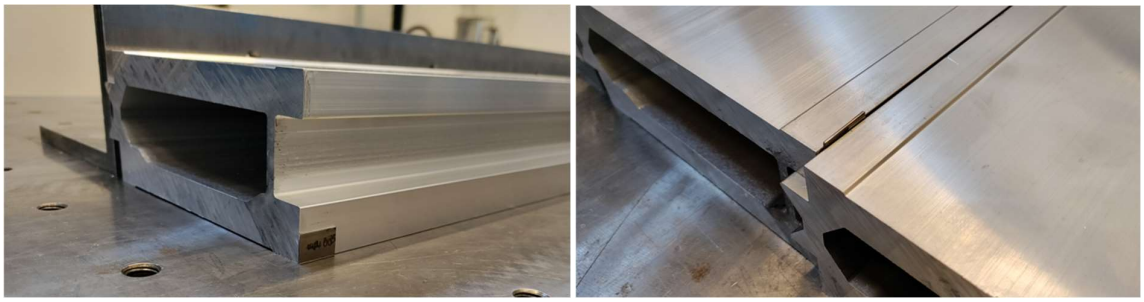

(a) **(b)**

Figure 18: Steel spacer inserted at (a) the bottom of profile and (b) the top of profile

Blade gauges were used to check the consistency of the gaps throughout the length of the weld seam, and any possible adjustments were made using pressure from the lateral bolts in the side rail. The gap was recorded at the center and each end. The 17 mm thick butt-joint was welded at all gap levels with the welding program re-written each time to start with the center the pin in the center of the gap. This method was decided upon to standardize the results due to limited material resources available for welding experiments. Each resulting weldment was labeled accordingly as: 0_Gap_17mm, 1_Gap_17mm, 1.5_Gap_17mm, 2_Gap_17mm, and 3_Gap_17mm, correlating with their gap level and material thickness. The resulting flash was cut away using, a milling machine, to provide a level surface on the workpiece to prepare for welding on the 23 mm side. The weldments were flipped over, and the process is repeated. Because the welded profiles were found to be bowing upward towards the center, two additional vertical clamps were added in the centers for welding the 23 mm side, as can be seen in Figure 19. The resulting 23 mm thick welds are labeled as: 0_Gap_23mm, 1_Gap_23mm, 1.5_Gap_23mm, 2_Gap_23mm, and 3_Gap_23mm. The blade gauges were used post-weld to measure the gap levels of all welds, on the unwelded portion at either end of the weldment, and the measurements were recorded.

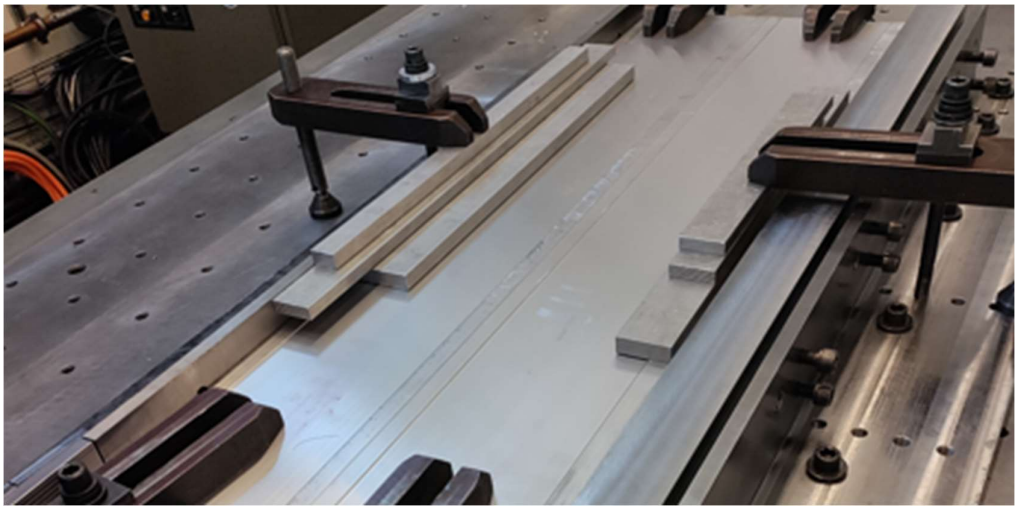

Figure 19: Vertical clamps added to center of profile to reduce bowing

3.3 Sample preparation

3.3.1 Sawing

The initial cutting of the welded profiles was performed, at using a Salvador Classic 50 crosscut saw. This step also took place at Hydro Innovation and Technology in Finspång, Sweden. A total of six cuts were made on each weldment which resulted in seven separate pieces, as can be seen in Figure 20.

Figure 20: Profiles sawed into sections post-welding

The start and finish of each weld were removed at 140 mm from each edge of the weldment. Three sections of 30 mm lengths were taken from the start, middle, and end of each of the remaining welds for macrographic examination. Two sections were cut at 310 mm lengths. Due to time limitations, only the 310 mm section closest to the end of the weld is to be used for extracting tensile testing specimens. Each section was marked, using a pneumatic engraving pen, with an identifier containing the gap level, weld thickness, and where the section came from within the weld. A closer view of the measurements of each section and engraving can be seen in Figure 21.

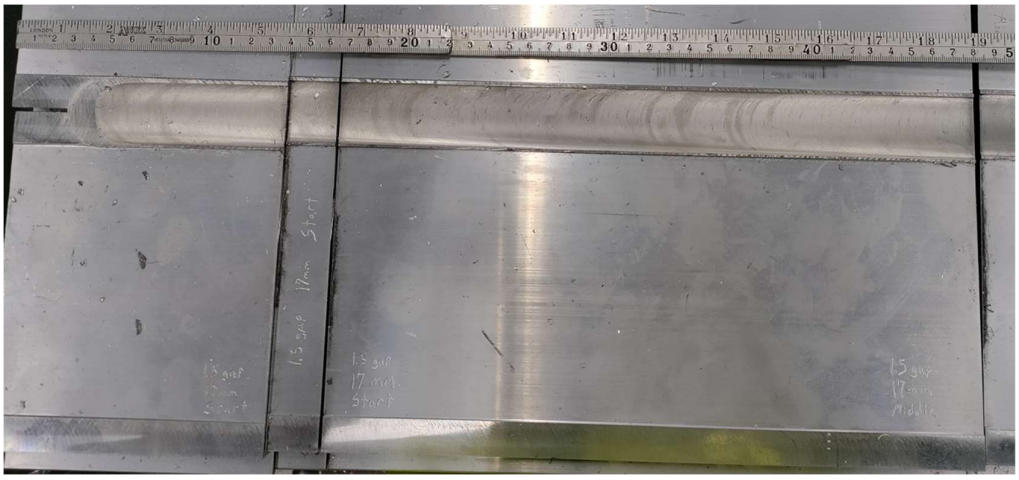

Figure 21: Measurements of sawed sections with visible engraving

3.3.2 Macrographic examination samples

The 30 mm long samples remained at Hydro Innovation and Technology in Finspång, Sweden to be prepared for macrographic examination.

3.3.3 Tensile sample preparation

The 310 mm long sections were shipped to SINTEF in Trondheim, Norway. There they were split in half, separating the 17 mm welded side from the 23 mm welded side, to prepare for machining out the tensile specimens.

The CNC machining to prepare the specimens was done at Cycle Start AS in Barkåker, Norway. Each section had five units machined out of it to accommodate four tensile sections spaced evenly throughout each 310 mm long section. An example of a 310 mm section, post-CNC machining, can be seen in Figure 22.

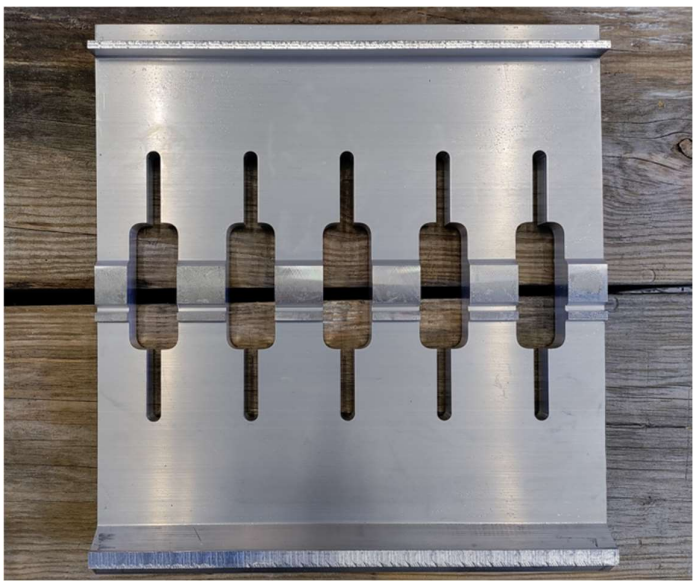

Figure 22: 310 mm profile section after CNC machining

The sections were then returned to SINTEF in Trondheim, where two final cuts were made on each section, with a band saw, to release the specimens. A dimensioned drawing of the 17mm weld thickness tensile specimen's general geometry can be seen in Figure 23. It should be noted that though the weld thickness is 17 mm, there is a 1 mm high section built up only in the area, which is underneath of the welding shoulder, as can be referenced from Figure 15 in section 3.1.2. This build up is flattened out during welding and the remaining wall thickness of the cross-section is 16 mm, as can be seen in Detail A of Figure 23. The same applies towards the 23 mm weld thickness specimens, which has the same general geometry as seen below, outside of the cross-sectional thickness which is measured as 22 mm after welding.

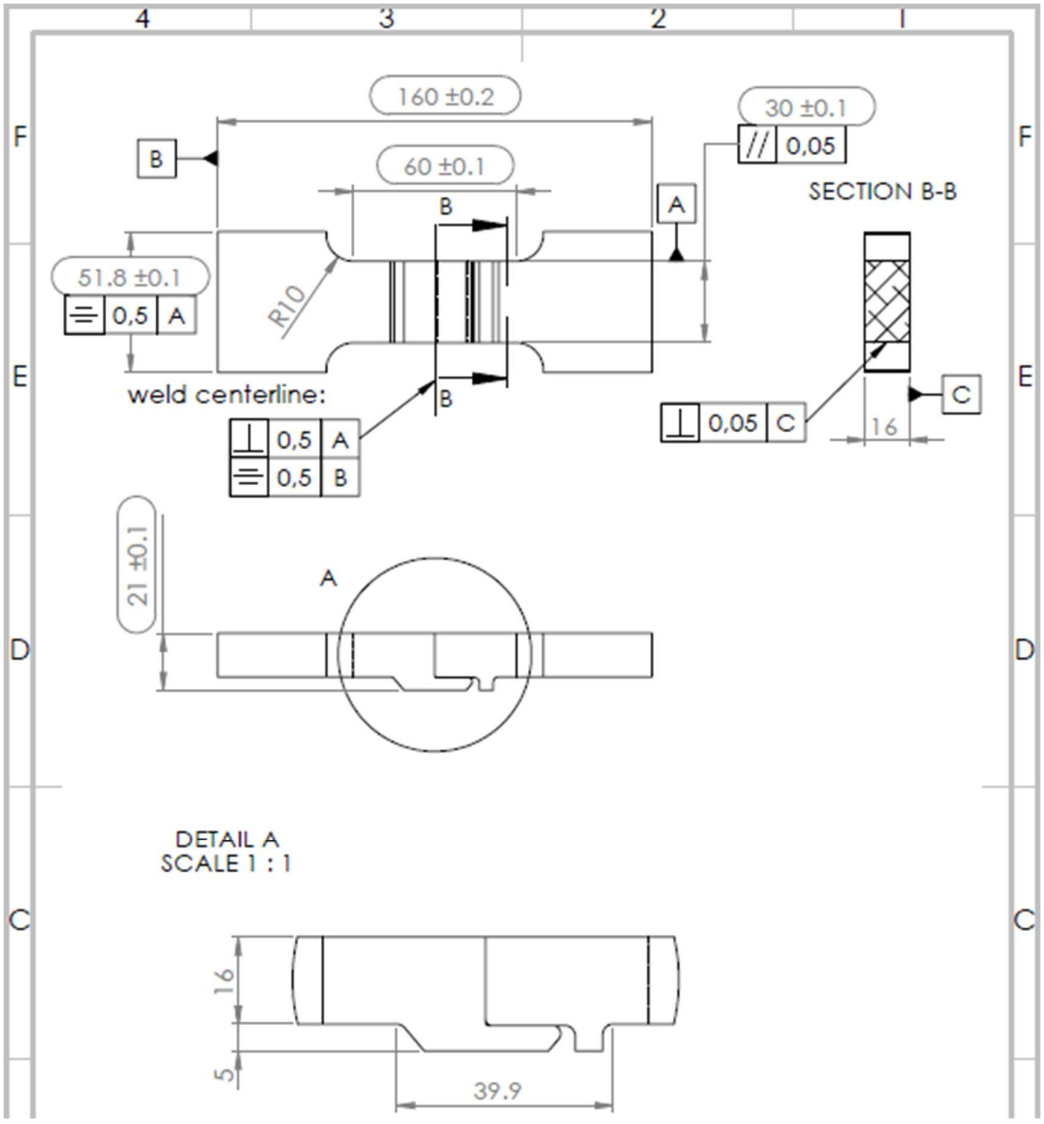

Figure 23: Dimensioned drawing of 17 mm weld thickness tensile specimen

The specimens were labeled with the weld identifier and an additional individual identifier of 5, 6, 7, or 8 to track where it came from within the weld and identify changes in the tensile strength throughout the progression of the weld. The identifier 5 is the first in the section and 8 being the end specimen.

3.4 Testing

3.4.1 Macrographic examination

The macrographic examination was performed using standard procedures at Hydro Innovation and Technology in Finspång, Sweden.

3.4.2 Tensile testing

The tensile testing was performed on an Instron Multiaxial 250 kN test machine NTNU in Trondheim, Norway. A displacement rate of 7.8 mm/min was used for testing. For the purposes of calculating UTS, the area of 16x30 mm² and 22x30 mm² are used for the 17 mm and 23 mm thickness welds, respectively. This is chosen as the region of fracture is through only the single wall thicknesses of 16 mm and 22 mm which were discussed in section 3.3.3, and the gauge width is 30mm. While there may be some variation in the thickness of these cross-sections due to left over welded material in the shoulder affected zone, which could slightly affect the accuracy of the UTS calculations, it is viewed as sufficient for comparisons within this thesis. Each specimen was recorded in regard to the side and zone within the weld at which the fracture occurred.

14 specimens were tested for the 17 mm thickness welds, and 16 specimens for the 23 mm thickness welds. Because of the void defects, the welds with 3 mm gap width were not part of the tensile test as they would not have passed inspection in a production scenario with the voids being visible from the exit hole. The number of specimens for which results were recorded for each gap level at each weld thickness can be seen in Table 9. The 1_Gap_17mm_No7 and 2_Gap_17mm_No7 tensile results were lost in error, with no usable data output from the tensile machine.

Table 9: Number of tensile specimens at each weld thickness and gap level

17 mm welds		**23 mm welds**	
Gap Width	Num. of Specimens	Gap Width	Num. of Specimens
0 mm	4	0 mm	4
1 mm	3	1 mm	4
1.5 mm	4	1.5 mm	4
2 mm	3	2 mm	4

4 Results and Discussion

In the following sub-sections, the results from the experimental segment of the thesis will be presented. Section 4.1 will present the observations made during fit-up, welding of the profiles, and post-weld. Section 4.2 will show and discuss the results of the macrographic cross-sections of each weld. These cross-sections will be discussed with relation to the welding forces and torque output from the welding machine. Section 4.3 will display and discuss the results from the tensile testing.

4.1 Welding observations

4.1.1 Fit-up of profiles/gap consistency pre-weld

There are several form factors which are given tolerances in the EN755-9 standard which apply to the pre-weld fit-up of these aluminum profiles. Straightness tolerance within this standard, as mentioned before, shall not exceed 1.5mm/m length and local deviations shall not exceed 0.6mm/m length. Profiles which are out of tolerance in straightness will have a bow in the length of the profile, which will either cause an unwanted gap in the center of the fit-up or on either end. One profile was not flat and was discarded due to problems with fitting together with the other profiles. Disregarding the profile, which was discarded, the profiles used in this study were able to satisfy this straightness requirement over 1-meter of length for the purposes of this experimentation. This means that they were either straight enough from the extrusion line or were able to be pressed into compliance by adjusting the bolts in the side rail in the experimental setup.

Though they were able to be forced into compliance, some deviations in straightness affected the experimental results with regard to pre-weld fit-up. The pre-weld gap measurements showed that the gap near the center of the profiles tended to deviate from the gap near the edges of the profiles. To produce the desired gap level at the ends of the weld, the gap in the middle could not be totally controlled. When attempting to produce the 0_Gap_17mm weld, the pressure from the side rails was enough to compensate for any bow within the profiles, without the use of excessive force. The gaps at the 23mm weld thickness level experienced shrinkage of the gaps in both the ends and the center of the gap length, after having been welded on the 17mm side. The gap reduction was more prominent towards the center of the welds. This is thought to be from the cooling of the welds causing shrinkage without a spacer in the center to keep the distance set. The pre-weld gap measurements can be seen in Table 10. The data for the 17 mm weld thickness pre-weld center measurements is missing for this table. These measurements are anticipated to follow the trend of the profiles having a minor bow towards the center, which will make the center gap measurements slightly smaller than the ends near the spacers.

Table 10: Pre-weld gap measurements

Pre-weld measurements						
	17 mm			23 mm		
Weld	Start	Mid.	End	Start	Mid.	End
0 Gap	x	x	x	x	x	x
1 Gap	1.0	0.8	1.0	1.0	0.7	1.1
1.5 Gap	1.5		1.5	1.4	1.0	1.5
2 Gap	2.0		2.0	1.9	1.3	2
3 Gap	3.0		3.0	2.9	2.2	3

None of the produced gaps deviated at, or exceeding, the intended gap level over 1.5mm/m of length. The largest deviations are on the 2_Gap_23mm and 3_Gap_23mm welds. They deviated from the intended gap level, in the center of the fit-up, at 0.7 and 0.8 mm, respectively. This does exceed the local deviations tolerance of 0.6mm/m of length, however these variations in gap level proved to be gradually changing over the length of the profile.

4.1.2 Widening of gap during welding

While welding along the length of each gap, a visible widening occurred in front of the tool's path of travel. Once the tool exited and the material began to cool, the gap would typically shrink down to, or slightly smaller than, the original size. This phenomenon occurred at every gap level but was more pronounced at wider gap levels. A visualization of this occurring during a 2 mm gap weld can be seen in Figure 24. It can be seen that the gap has nearly doubled in size in front of the tool during welding. After concluding the experimentation, it is not completely certain as to why this widening is taking place and where within the profile or fixture is allowing this flexibility of the gap width during welding. As one side rail is completely stationary, and the other has components for lateral adjustment, it is reasonable to assume some flexibility within the adjustable area of the siderail. During the experimentation, the goal was to keep a consistent gap between the profiles, and due to some inconsistencies in the profiles resulting in reduced gap width, some areas of the adjustable side rail was not tightened with force as this would have closed the gap beyond what was wanted. This will raise some uncertainty in the results, as the gap at the point of the tool during welding may be pushed larger than what is intended and recorded.

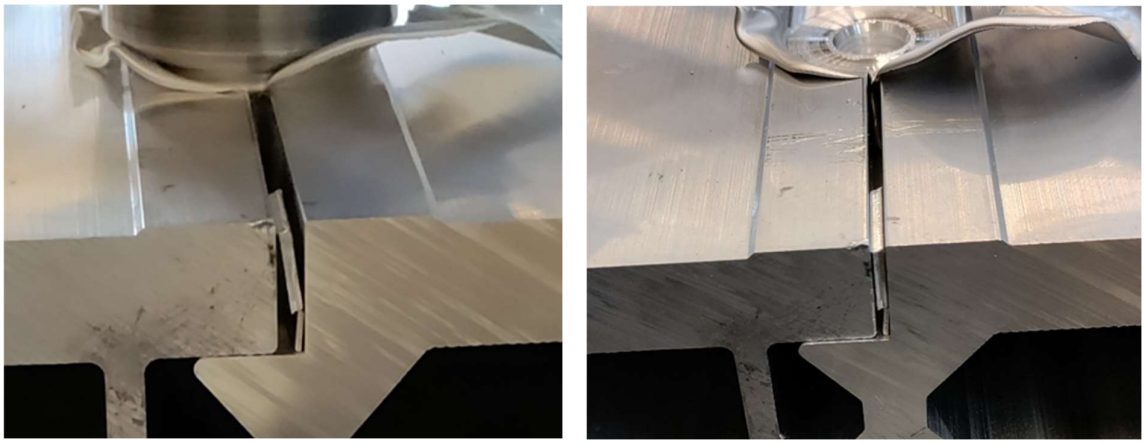

(a) **(b)**

Figure 24: During welding, (a) widening of gap in front of tool and (b) gap shrinking upon cooling

In some of the cases the gap, at the point between the spacer and the end of the weld would compress and shrink beyond the width of the spacer of the spacer. The measured decrease of the gap widths was more prevalent at the end of each weld than the beginning. The severity of shrinkage was the highest at the widest gap levels of 2 and 3 mm. The measurements of the gaps, on the unwelded portion near the starting and finishing ends of the weldment, can be seen in Table 11.

Table 11: Post-weld gap measurements

Post-weld measurements				
	17 mm		23 mm	
Weld	Start	End	Start	End
0 Gap	x	x	x	x
1 Gap	1.4	1.1	0.8	0.8
1.5 Gap	1.9	1.4	1.4	1.4
2 Gap	2.0	1.8	1.5	1.5
3 Gap	2.9	2.3	2.5	2.3

4.1.3 Flash

As the widths of the gaps increased, the amount of material lost due flash increased as well. This loss of material became considerable for both the 17 mm and 23 mm thickness welds at the widest gap levels. The flash on the AS was continuous and exited the weld path in one spiraling length. The flash on the RS was to a lesser extent than on the AS but was proportional to and indicative of what was exiting the weld on the AS. The flash on the RS was left stationary on the edge of the weld. An example of the increase in flash on the RS for the 23 mm thickness welds, as well as an example of the AS material loss for the 3_Gap_23mm weld can be seen in Figure 25.

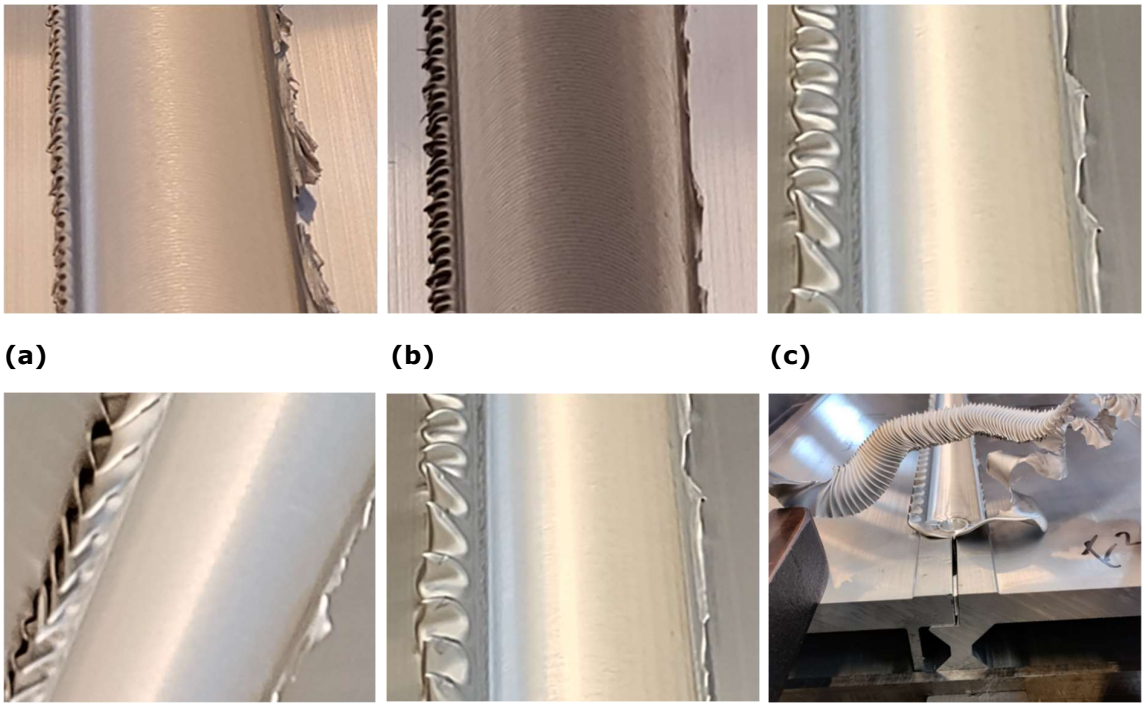

Figure 25: Flash on RS of 23 mm welds at (a) 0_Gap, (b) 1_Gap, (c) 1.5_Gap, (d) 2_Gap, (e) 3_Gap, and (f) AS material loss on 3_Gap

During the welding process, small adjustments were made to the Z-axis position were made in an attempt to rectify the amount of flash the welding process was creating at the 3 mm gap level. It can be seen, in Figure 26, that during the 3_Gap_17mm the operator raised the Z-axis position at 400 mm into the length of the weld because of the excessive flash being created on the AS.

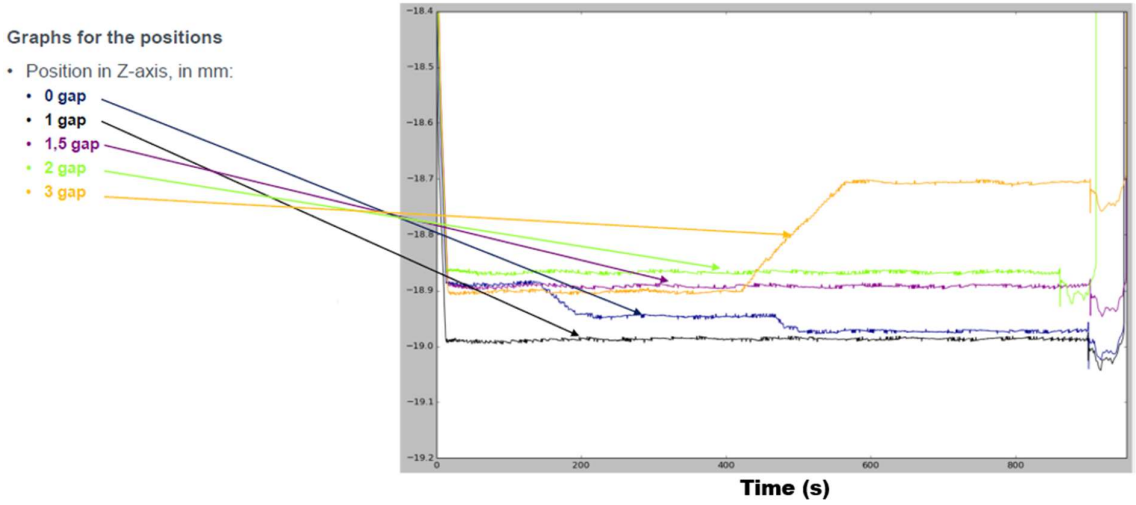

Figure 26: Adjustments made to Z-axis position during 17 mm thickness welds

Similar adjustments were made during the 23 mm weld thicknesses. It can be seen in Figure 27, that because of the large amount of flash created during the 3_Gap_17mm weld, the 3_Gap_23mm was started with a raised height from the beginning of the weld.

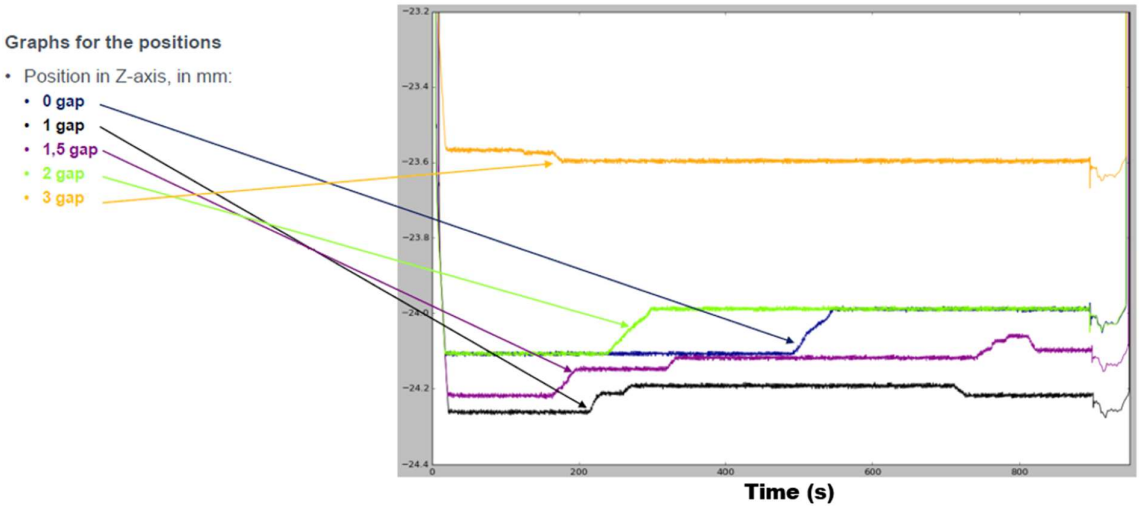

Figure 27: : Adjustments made to Z-axis position during 23 mm thickness welds

4.1.4 Surface defects

The initial visual inspection of the welds showed that the FSW process was able to successfully weld gap levels of 0.0, 1.0, 1.5, and 2.0 mm, on both the 17 mm and 23 mm sides, with without any visible surface defects or defects visible from the exit hole. On the 3_Gap_17mm weld, a void can be seen on the advancing side from the exit hole, as is shown in Figure 28. Though there was a void visible in the exit hole, this weld did not show any visible surface defects along the length of the weld.

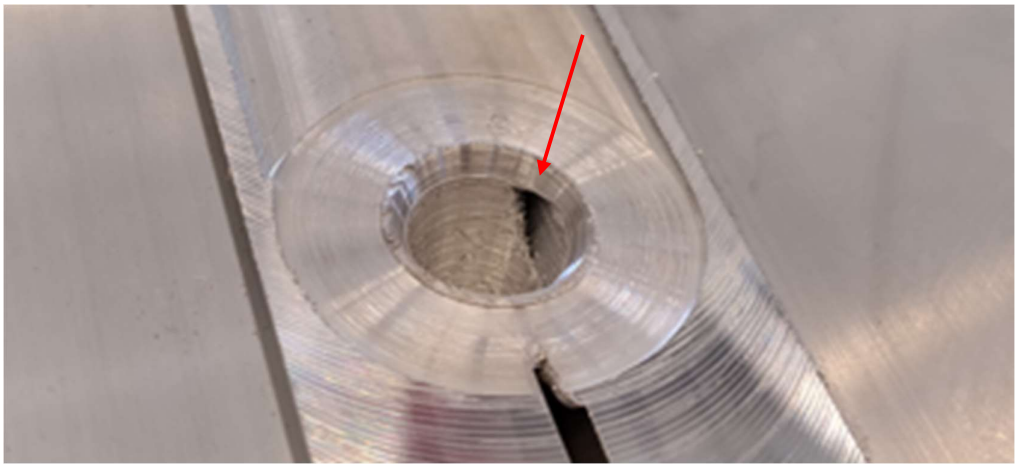

Figure 28: Void visible on the advancing side of exit hole on 3 Gap 17mm weld

On the 3_Gap_23mm weld, a void is again visible from the exit hole. Also, surface lack of fill defects can also be seen in the beginning and end of the weld, but not in the middle. This is shown in Figure 29. This lack of any surface defects in the middle can feasibly be explained by referring back to the pre-weld gap measurement distribution for this weld in section 4.1.1. This weld had a gap of 2.9 mm at the start of the weld and 3.0 at the end

of the weld, both of which regions experienced the surface lack of fill defect visible on the surface of the weld. Due to inconsistencies in the straightness of the profiles, this gap gradually decreased to 2.2 mm at the center of the weld where there is no defect visible at the surface.

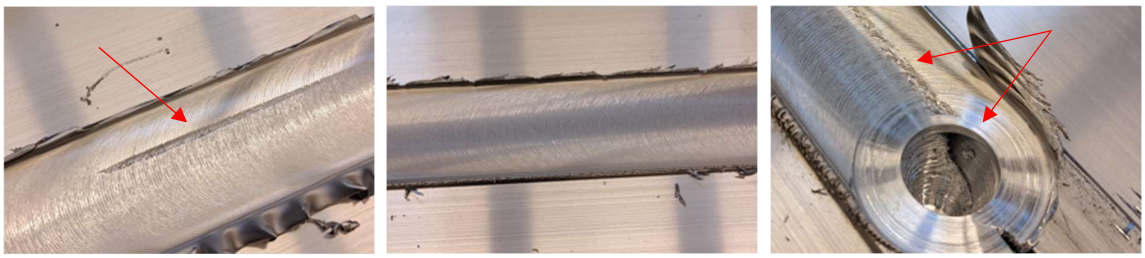

(a) **(b)** **(c)**

Figure 29: 3_Gap_23mm weld showing (a) surface lack of fill defect at beginning of weld, (b) sound surface qualities in the middle, and (c) surface lack of fill defects and visible void on advancing side at the end of weld

4.2 Macrographic examination with welding forces and torque analysis

This section will display the macrographic examinations of each weld and discuss the relating forces and torques experienced during the welds. As there are large oscillations and many data points, the averages, maximums, and minimums of the forces and torque are approximations based on measurements taken from within the graphs. This is meant to identify any trends within the forces and torque as the gaps in the welds progress. The forces are measured within the spindle of the welding machine, following a Cartesian coordinate system with X representing the direction of the weld, Y representing perpendicular to the weld, and Z representing up and down. When measuring the forces and torque, welding is beginning when the Z-axis line can be seen to reach its final depth and normalize. It should be noted that in all graphs that are to follow, the Y-force and Torque values are negative because of the nature of the direction of rotation during welding. A positive value can simply be substituted in their case. Because of the 1.5° tilt angle of the machine, the torque values start at a +21.5 Nm before rotation of the machine and then cross 0 and move into negative value. This gives the torque value a higher amplitude than initially appears in the graphs.

The 17 mm welds are presented first, followed by the 23 mm welds. A defined example of a cross-section showing the different zones of 2_Gap_17mm can be seen in Figure 30. This can be used for reference when discussing the cross-sections which are to follow.

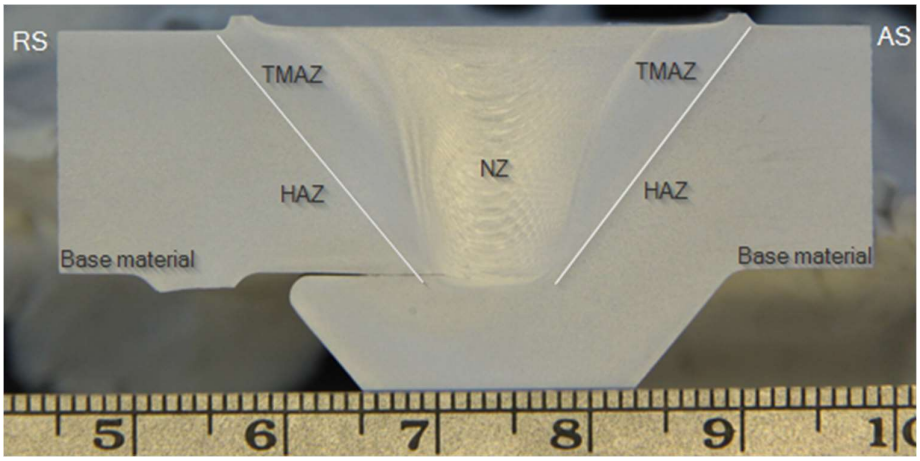

Figure 30: Defined view of 2_Gap_17mm weld

4.2.1 17 mm thickness weld results

The 0_Gap_17mm run produced sound welds throughout the start, middle, and end of the 1-meter length. The welding parameters were established using this set up, thus establishing a baseline to compare the welds to as the gaps become wider. The macrographic photos of these welds can be seen in Figure 31. Each section of the weld shows good material flow towards both the AS and RS as well as good root penetration. The NZ is well defined, tapered in the shape of the pin, and appropriately symmetrical about the centerline of the weld. The TMAZ is evenly distributed around the NZ and underneath the width of the shoulder. This weld experienced minor material loss due to flash, as discussed previously. The cross-sections of the weld show no discernible loss of volume in the weld, as is evident by the remainder of material still visible at the top of the weld, and lack of sagging in the weld.

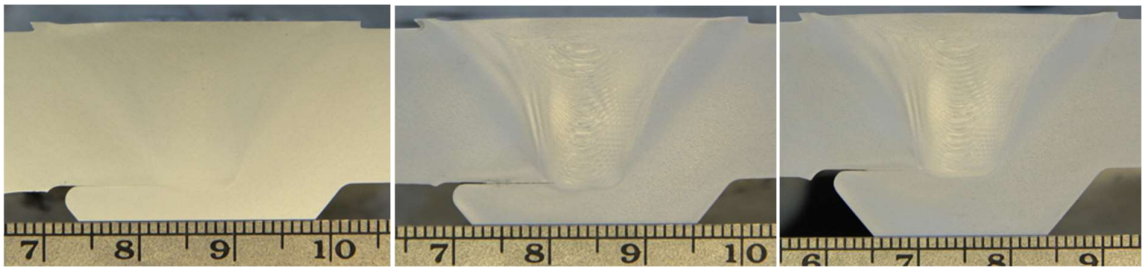

(a) **(b)** **(c)**

Figure 31: 0_Gap_23mm weld macrography at (a) start, (b) middle, and (c) end

During the 0_Gap_17mm weld the forces and torque experienced varied marginally across its extent. The average X-force experienced was approximately 5.7 kN. The maximum force experienced during steady state welding was 6.3 kN and the minimum was 5.0 kN, giving a variation of 1.3 kN across the length of the weld. The Y-force average was 2.5 kN with a maximum of 3.7 kN and minimum of 2.0, giving a total variance of 1.7 kN across the weld. The Y-force can be seen to oscillate during the weld, but also take a slight increasing overall trajectory from start to finish. The Z-force increases quickly to 40 kN and becomes moderately stable with a slight drop off before the tool exits. The torque is oscillating similarly to the X-force and Y-force. The average torque value is 138.8 Nm, with a maximum value of 143.3 Nm and minimum value of 134.3 Nm. This means the torque

oscillates across a range of 9.0 Nm during the weld. The forces and torque experienced during this weld can be seen in Figure 32, and this graph serves as a baseline to compare the remaining welds of 17 mm thickness.

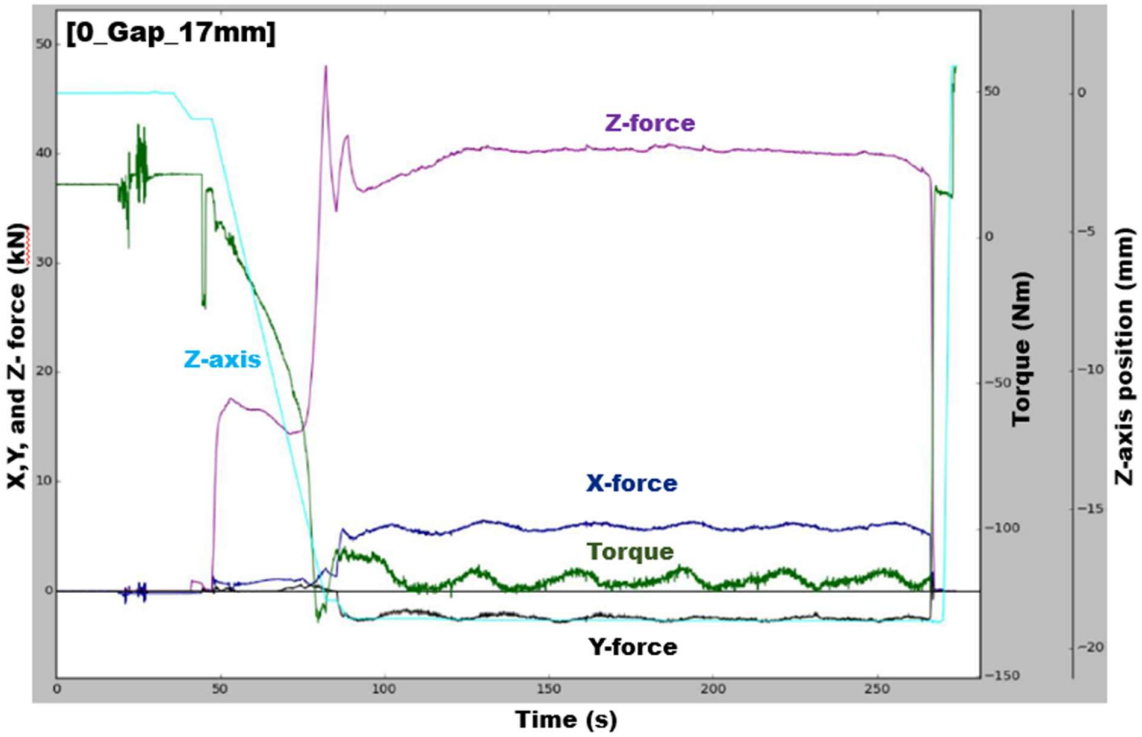

Figure 32: 0_Gap_17mm forces and torque

The 1_Gap_17mm weld again produces sound welds, with some minor changes when compared to the 0_Gap_17mm welds. The material flow is sound on both the AS and RS, and the NZ is again appropriately shaped and symmetrical about the centerline of the weld. With the introduction of a 1 mm gap, the TMAZ of the weld is still well defined, but is now reduced when compared to the 0_Gap_17mm weld cross-sections. The macrography of this weld can be seen in Figure 33.

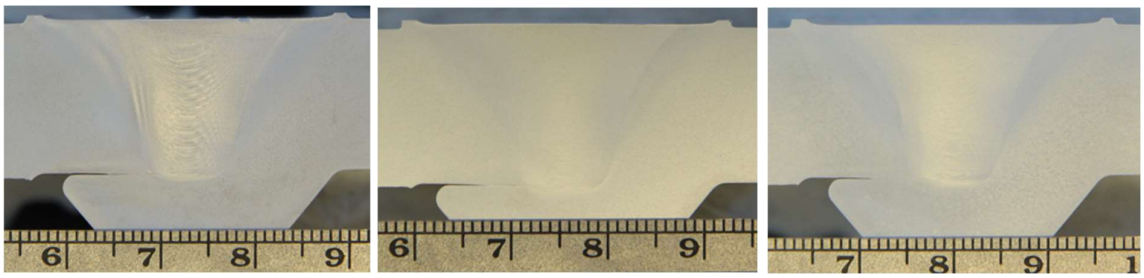

(a) **(b)** **(c)**

Figure 33: 1_Gap_17mm weld macrography at (a) start, (b) middle, (c) end

During the 1_Gap_17mm weld, the behavior and stability of most of the forces and the torque appears similar to that of the 0_Gap_17mm weld. However, there is a reduction in the average X-force experienced to 4.7 kN and an increase in the average Y-force to 3.5 kN. The average torque has reduced slightly to 134.7 Nm. The behavior of the Z-force is the most notable difference between this and the previous graph. The value is slightly

reduced to 35.2 kN, but the amplitude of change from the start, middle, and end is more severe. The Z-force varies by 5.7 kN throughout the weld, peaking near the center of the weld and then dropping again at the end. The forces and torque graph for the 1_Gap_17mm weld can be seen in Figure 34.

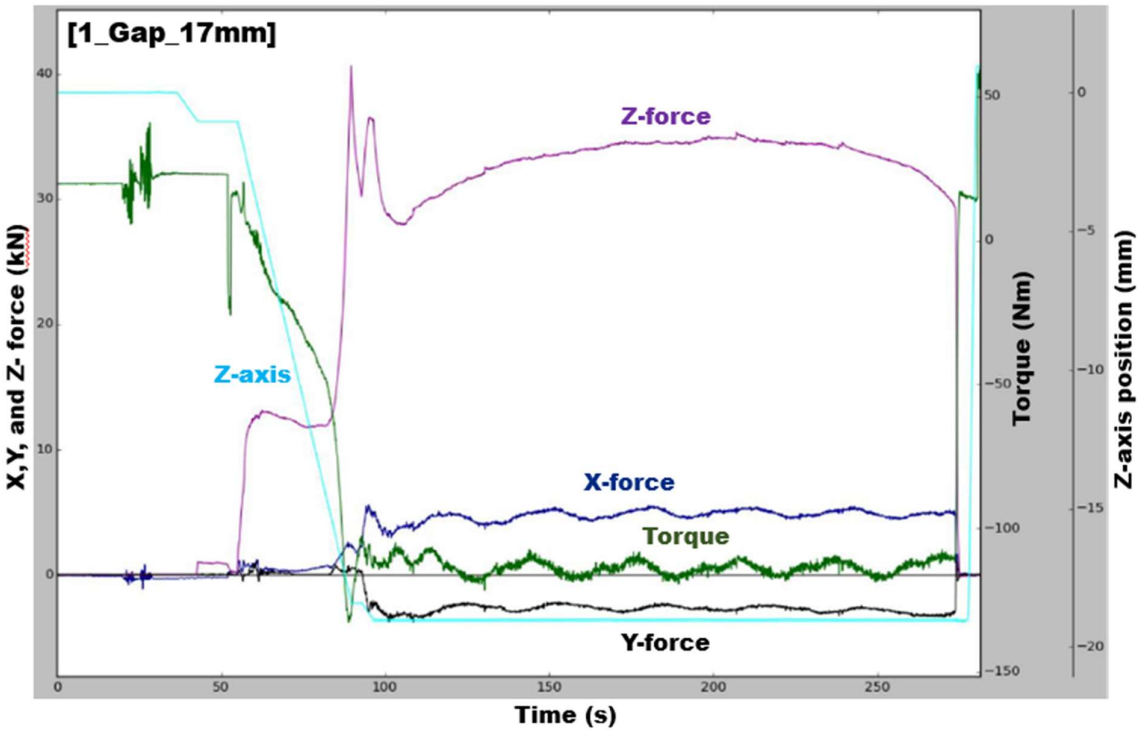

Figure 34: 1_Gap_17mm forces and torque

The 1.5_Gap_17mm, shown in Figure 35, weld produces cross-sections nearly identical to the 1_Gap_17mm weld. They appear sound and with little noticeable difference or reduction of the zones.

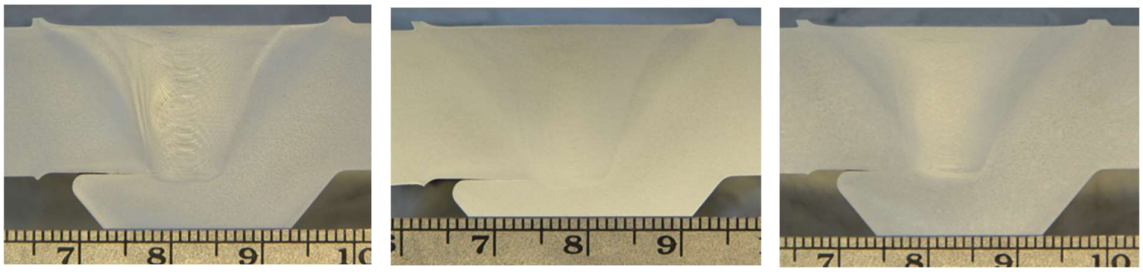

(a) **(b)** **(c)**

Figure 35: 1.5_Gap_17mm weld macrography at (a) start, (b) middle, and (c) end

During the 1.5_Gap_17mm weld, the forces and torque are continuing to show increasing instability. This shows a slight increase in the average X-force and torque when compared to the 1_Gap_17mm weld, which is in opposition of the changes seen previously. The average Y-force continues to increase slightly to 3.7 kN, and the Z-force reaches a similar maximum value. The Z-force again peaks in the center and then reduces, this time more sharply, varying 7.2 kN across the weld. The graphical output for the 1.5_Gap_17mm weld can be seen in Figure 36.

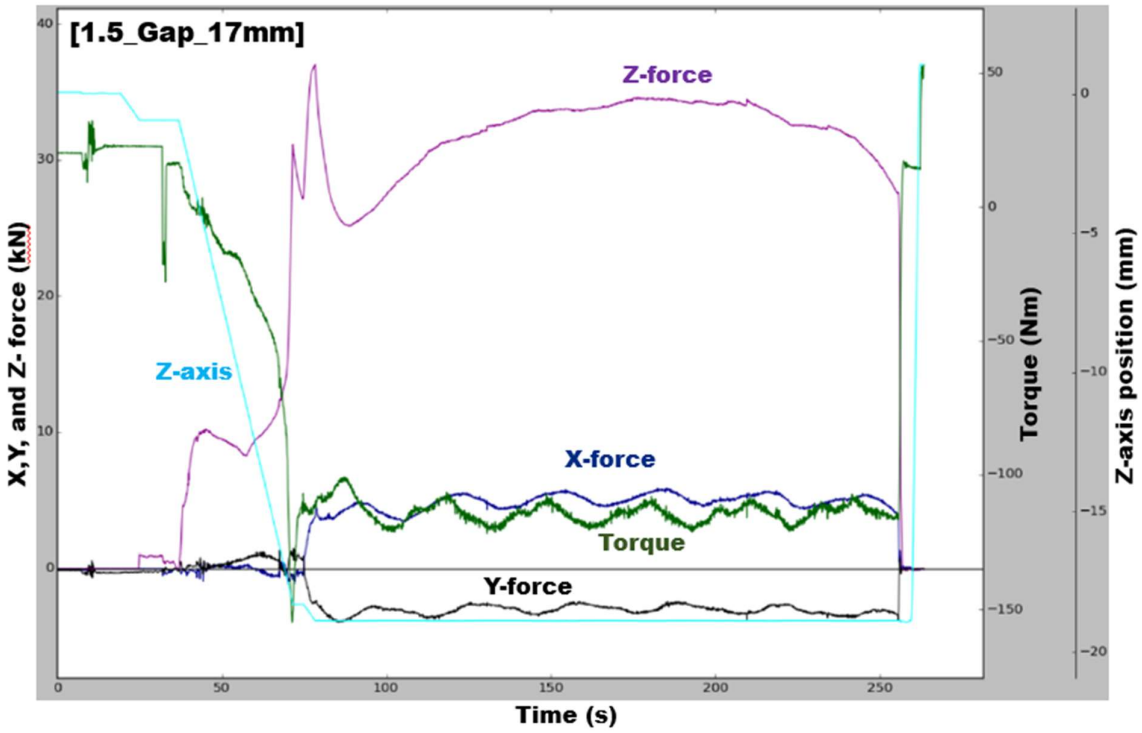

Figure 36: 1.5_Gap_17mm forces and torque

The 2_Gap_17mm weld continues to produce sound cross-sections. The edges of the NZ are beginning to look less robust, the change of the material's color in the TMAZ is less apparent, and the transition between zones is less defined than previous welds. The macrography for this weld is shown in Figure 37.

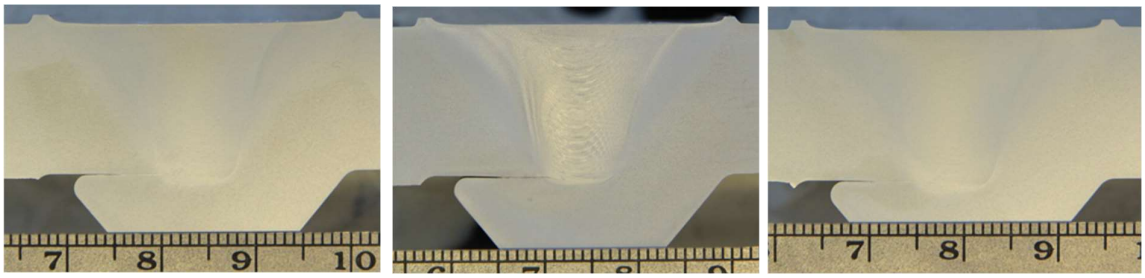

(a) **(b)** **(c)**

Figure 37: 2_Gap_17mm weld macrography at (a) start, (b) middle, and (c) end

During the 2_Gap_17mm weld, the average X-force returns to its decline to a value of roughly 4.0 kN and shows similar behavior as the previous welds. The average Y-force value rises to 4.3 kN and also shows the same behavior and oscillation as it has with the previous welds. The Z-force drop reaches a lower maximum value of 30.8 kN and shows similar behavior and variation from throughout. The average torque returns to a decline at 133.6 Nm, as shown in Figure 38.

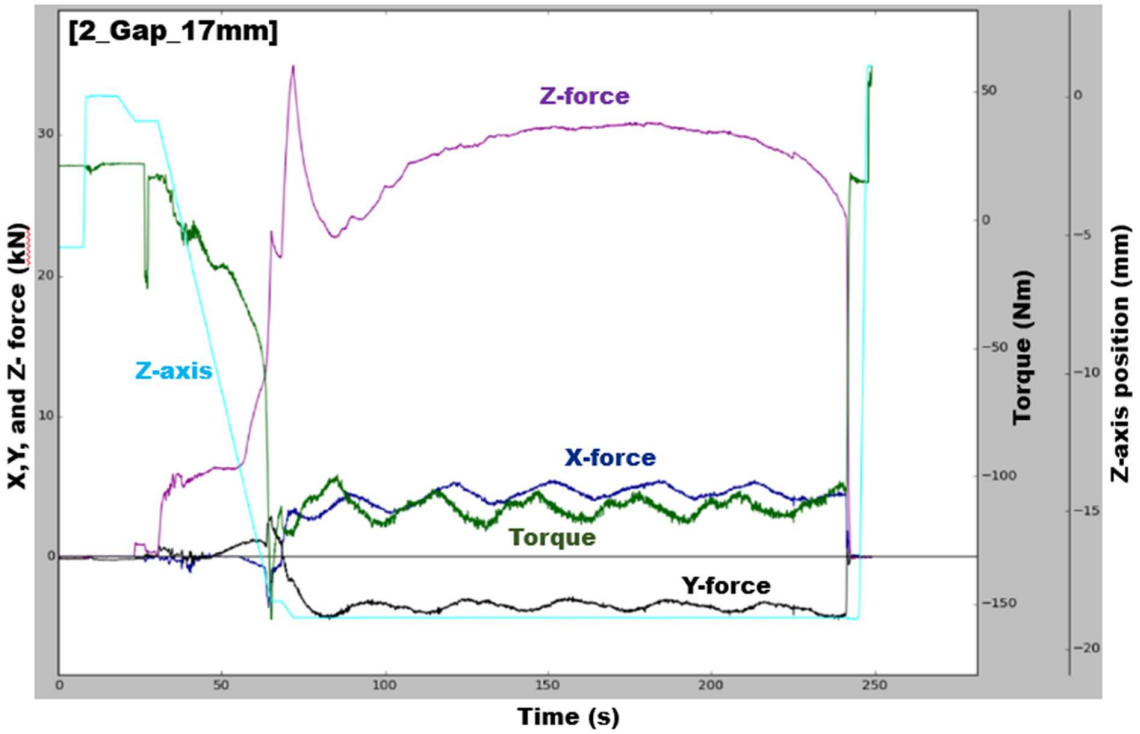

Figure 38: 2_Gap_17mm forces and torque

At the 3.0 mm gap level, voids within the weld become apparent on the AS within the NZ. For the 3_Gap_17 mm weld, the void is found in the start, beginning, and end of the weld as can be seen in Figure 39. The size of the void is largest at the beginning of the weld, smaller in the middle, and slightly larger again at the end of the weld. In the cross-sections for this weld, the upper area of the NZ is noticeably less wide, and the top of the weld begins to sag. The color change in the TMAZ is reduced, especially on the AS where the voids are found.

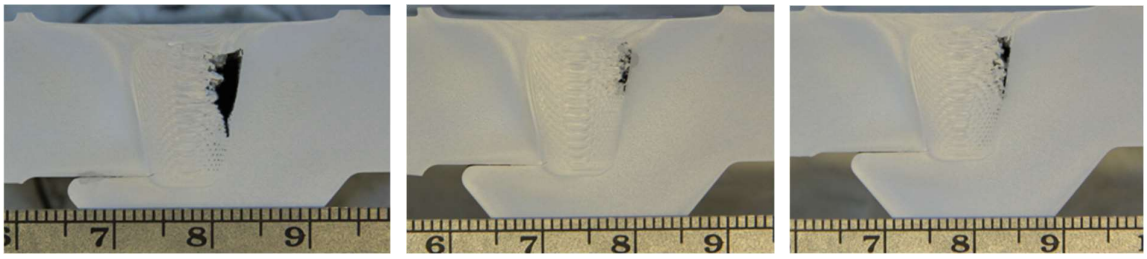

(a) **(b)** **(c)**

Figure 39: 3_Gap_17mm weld macrography at (a) start, (b) middle, and (c) end

The 3_Gap_17mm weld shows a good amount of instability in the forces and torque. The average X-force drops again to 3.3 kN and oscillates throughout the weld, varying by an amplitude of 2.8 kN. The average Y-force shows a large increase to 6.0 kN and the average torque drops to 126.6 Nm. The average Z-force is much lower at 18.0 kN and does not show similar behavior to the previous welds as it is fairly level throughout, except for one large spike at roughly 140 seconds into the weld. This spike in the Z-force correlates with a spike in the torque, a large reduction in the Y-force, and a small increase in the X-force

as it was on a downward trajectory. The forces and torque for the 3_Gap_17mm weld can be seen in Figure 40.

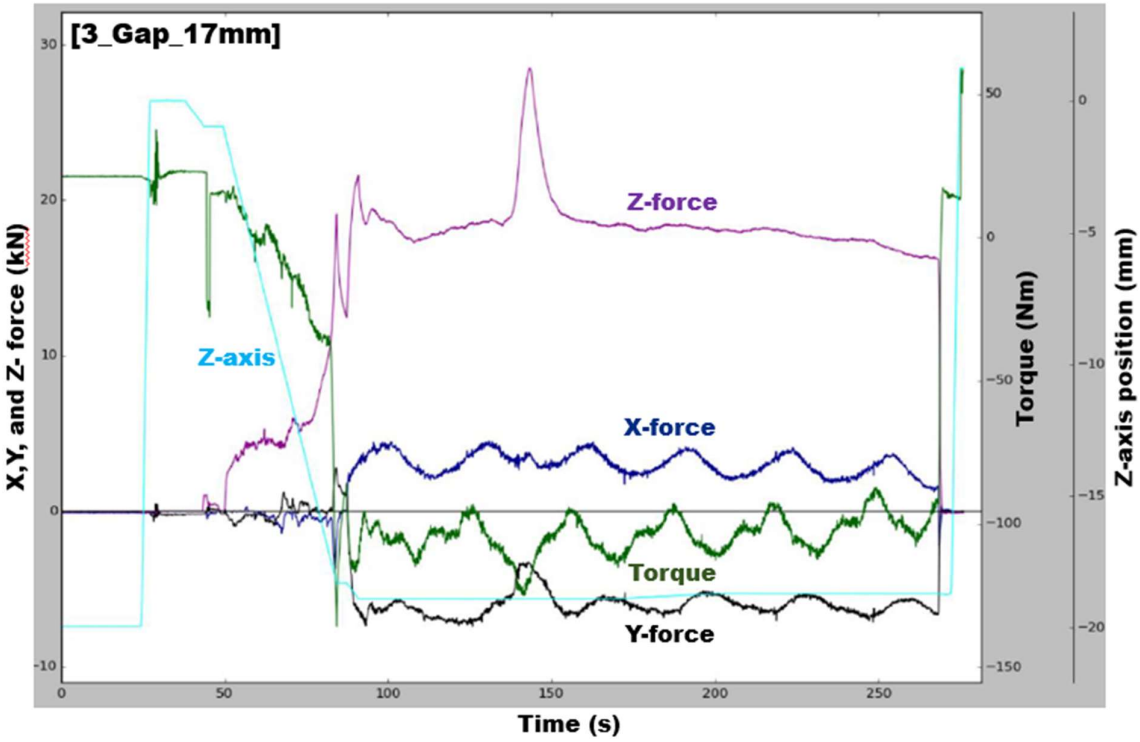

Figure 40: 3_Gap_17mm forces and torque

4.2.2 17 mm thickness welds discussion

Looking at the progression of the graphs in the previous section, it is evident that as the welding gaps grow larger, the amplitude of variation experienced in the form of forces and torque become increasingly unstable. Looking towards trends may help identify a window within which the force and torque parameters must be located to produce defect free welds. The variation of the average resulting forces and average torque across the progression of gap levels can be seen in Figure 41.

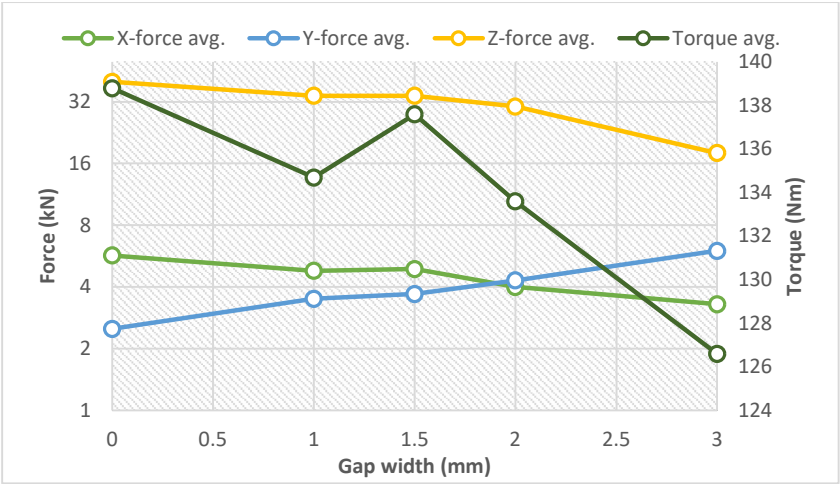

Figure 41: Average forces and torque for 17 mm weld thickness

As the gap levels get larger, it has been shown that the X-force is decreasing. As discussed in section 2.5, in the presence of a larger gap, there is less surface area for which the pin and shoulder are in contact with. Less surface area for the pin and shoulder to rotate against, in theory, indicates less friction and thus less heat creation. With less heat creation the material will not be as soft, and the flow stress will be increased, causing more resistance forces when traversing along the X direction. Typically, lowering resulting forces experienced in the X direction would be indicative of higher heat creation and in turn, softer material, less flow stresses, and less resistance towards advancement. The torque values lowering as the gaps get wider would also support the idea of higher heat creation, as the material would be softer and require less torque to rotate material around the pin and beneath the shoulder. However, as the gaps grow, the lowering Z-force value is in contradiction to this, as the downward forging pressure is responsible for a large portion of the heat generation within FSW. The reduction in the width of the TMAZ, at wider gap levels, is also in contradiction with the idea of higher heat creation. The lowering of the X-force and torque at higher gap widths is more likely to be due to lack of resistance because of the vacancy of material in the gap than it is to be resulting from the effects of higher welding heat, as this would typically indicate.

As was discussed in section 4.1.2, when welding in the presence of a gap, it was noticed that the profiles were being pushed apart in front of the tool. This is a possible explanation for the lowing of the X-force as the gap width grows. The profiles being pushed apart could be reducing the forces acting against the tools in the X direction. The fact that the Y-force is inversely growing as the gap widens could be the forces acting upon the tools as the side rail pushes back against the separating profiles in the Y-direction. It is worth noting that for the 2_Gap_17mm weld and 3_Gap_17mm welds, the Y-force values were higher than the X-force values. Somewhere within the welding set up, flexibility or movement is being allowed where it shouldn't. This could also be the nature of the profiles, as they are hollow, and the complex geometry allows more points which could be allowing flex. Extra clamping, as was added to combat bowing as shown in section 3.2.2, could have benefited the 17 mm thickness welds. This will have a dampening effect on the profiles throughout the greater middle region of the weld where vibration is likely occurring as the profiles are hollow and clamped only near their ends. This would also add extra assistance in the preventing the profiles from flexing or moving apart in front of the weld tool. This could have an effect which would reduce the more extreme oscillations in the forces and torque and produce a more controlled weld. As was stated in section 4.1.2, there was not a high amount of lateral force placed on the profiles, in an attempt to preserve the width of the gap in the middle. In a production environment the profiles would be pressed together with a much higher force, likely eliminating these issues experienced in this experiment.

As the gap level widens, the amount of remaining material underneath the path of the shoulder is decreasing. This is due to the increasing amount of material which is required to fill the vacant area in the presence of the gap. As mentioned in section 4.1.3, as the gap widths grow larger, the amount of material which was lost due to flash increased as well. The progression of the macrographic photos, in the previous section, show slight volumetric reduction of the welds especially noticeable at the end of the weld. This is apparent by the gradual decrease in remaining material at the top of the welds, as can be seen as the welded gap increases from 0 to 3 mm for the 17 mm weld thickness. This decrease in volume is expected and at gap levels of 2 mm and below there are no visible defects created due to lack of material. During the 3_Gap_17mm weld, this combination of the large amount of material lost in flash and the larger volume of vacant area within the gap led to voids within the weld. The very low Z-forces in the 3_Gap_17mm weld likely

contributes to the lack of heat and voids within the welds, as well. The Z-axis position was raised during this weld, as mentioned in section 4.1.3, to combat the excessive material loss due to flash.

4.2.3 23 mm thickness welds results

The 0_Gap_23mm weld produced sound welds with appropriately shaped NZ, symmetrical about the center of the weld. The TMAZ is clearly defined, and the material flow is good on both the AS and RS. There is no discernable loss of weld volume that can be seen from the start to the end of the weld. The macrographic examination of this weld can be seen in Figure 42. As the weld conditions are ideal and parameters designed for this set up, this again will serve as a baseline in which the other 23 mm weld thickness cross-sections can be compared with.

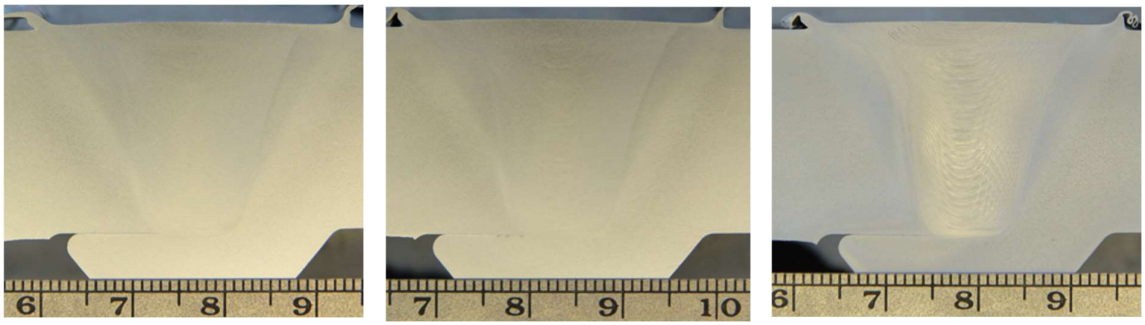

(a) **(b)** **(c)**

Figure 42: 0_Gap_23mm weld macrography at (a) start, (b) middle, and (c) end

The forces experienced in the 0_Gap_23mm weld, shown in Figure 43, are varying moderately but are more controlled than that of its 17 mm weld thickness counterpart. The average X-force is approximately 8.8 kN with a high of 9.9 kN and a low value of 7.5 kN. This give the X-force a variance of 2.4 kN across the length of the weld with the higher values in the middle of the weld and the lower values at the edges. The Y-force has the higher values at either end of the weld and the lowest in the middle. They average Y-force experienced is 5.4 kN with a maximum of 6.4 kN and minimum of 4.3 kN making a variance of 2.1 kN across the weld. Similarly, to the 0_Gap_17mm weld, the Z-force is peaking around 41.3 kN and is flatter across the weld than what is typical when gaps are introduced. The torque in this weld is gradually building up to an average of 216.2 Nm, which it holds fairly steadily until a slight decrease at the end near where the spacer is located.

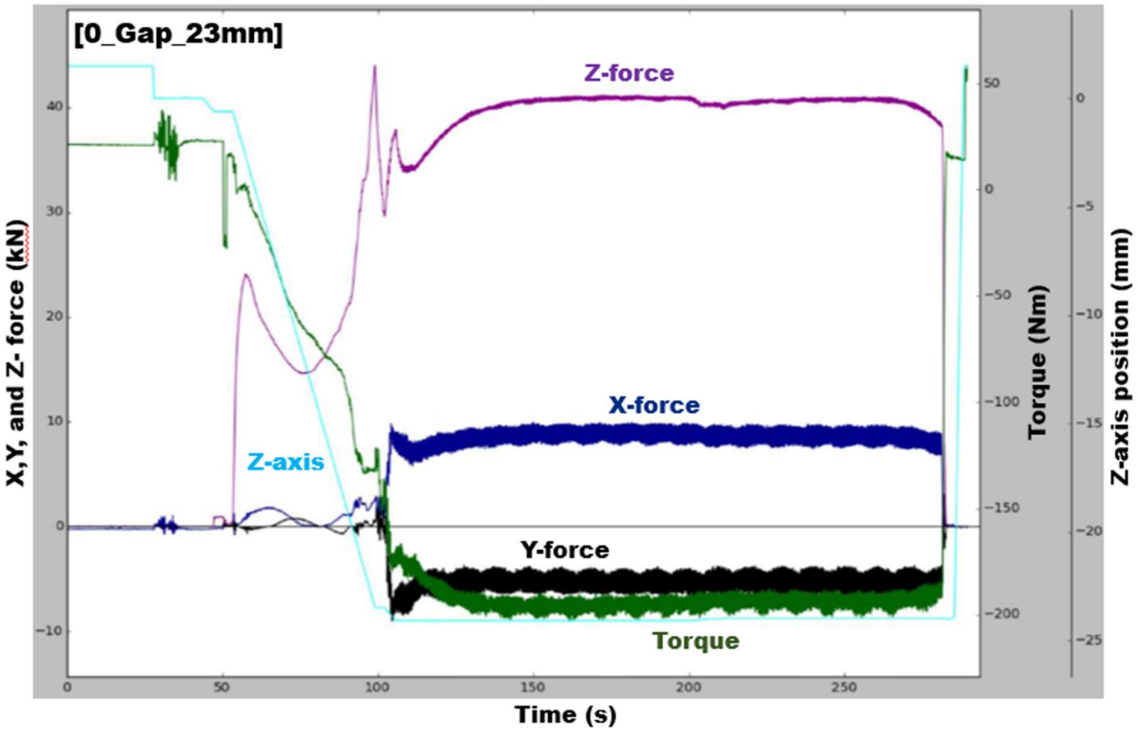

Figure 43: 0_Gap_23mm forces and torque

The 1_Gap_23mm weld shows sound symmetrical welds with well-defined NZ and TMAZ. In Figure 44, the TMAZ can be seen to reach out less widely in the start and end of the weld while remaining more robust in the center of the weld, pointing to higher heat generation in the middle of the weld. At the end of the weld, it can be noticed that there is a slight reduction in the remaining material at the top of the weld in the area of the shoulder.

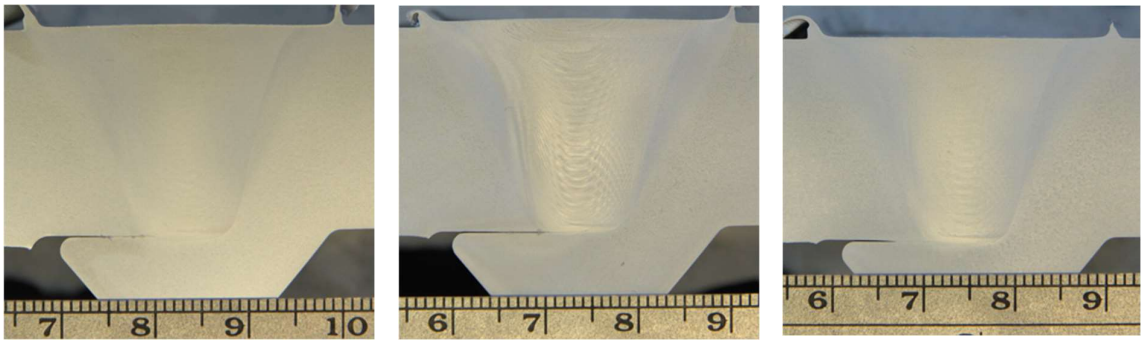

(a) **(b)** **(c)**

Figure 44: : 1_Gap_23mm weld macrography at (a) start, (b) middle, and (c) end

The forces in the 1_Gap_23mm weld are changing very little in behavior, outside of the Z-force, when compared with the 0_Gap_23mm graph. The average X-force drops to 7.9 kN with a higher variance of 4 kN across the weld. The average Y-force is 5.5 kN, also with a higher variance than the previous weld at 3.7 kN across the weld. The Z-force is now showing the more typical behavior in its arc, rising to a peak value of 38.8 kN and dropping to 30.3 kN at the end of the weld. The torque output is lower with the introduction of a gap, at an average value of 211.8. Again, the torque is lower near the edges where the

spacers are located, and higher throughout the majority of the weld in the center. The forces and torque for the 1_Gap_23mm weld can be seen in Figure 45.

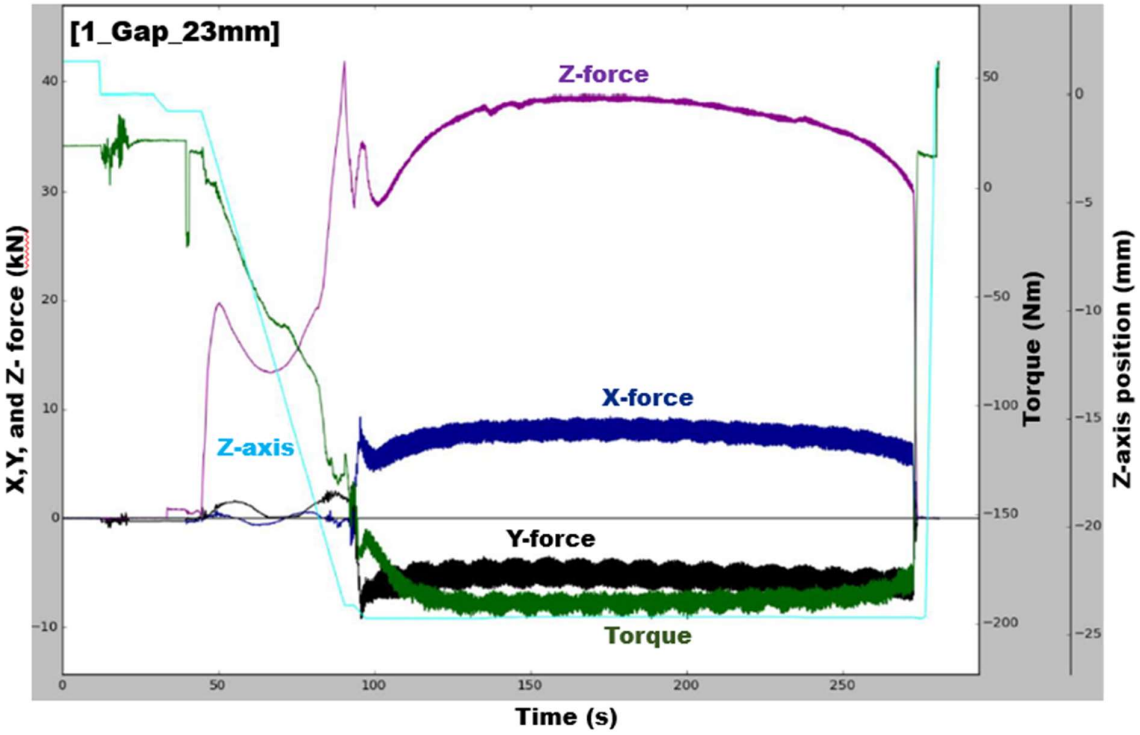

Figure 45: 1_Gap_23mm forces and torque

The 1.5_Gap_23mm cross-section shows a sound weld, but the TMAZ is again slightly less defines and not as robust as the previous welds. The RS of the weld is showing little definition in this regard towards the end of the weld. The top of the weld is showing excess material in the beginning and middle of the weld but is sagging in the center at the end of the weld. The macrographic examination of this weld can be seen in Figure 46.

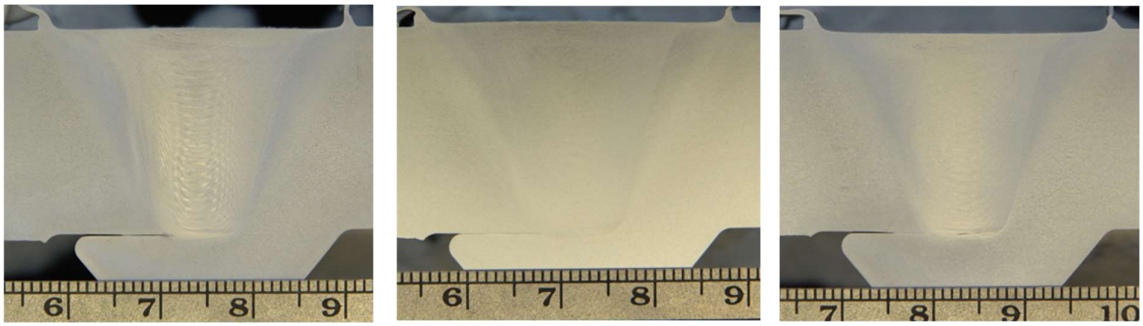

(a) **(b)** **(c)**

Figure 46: : 1.5_Gap_23mm weld macrography at (a) start, (b) middle, and (c) end

The forces in the 1.5_Gap_23mm weld, shown in Figure 47, continue the trend set previously. The X-force has dropped to an average value of 7.6 kN with a high of 9.0 kN and low of 4.1 near the end of the weld. The Y-force is noticeably tapering upwards throughout the end half of the weld after establishing an average value of 6.3 kN. The Z-force is producing a more extreme arc in this weld, with a peak value of 37.8 kN and a minimum value of 26.6 kN, giving an overall variance of 11.2 kN throughout the weld. This

is the largest variance of Z-force of any of the 23 mm thickness welds. The torque makes only a slight reduction from the previous weld to an average value of 210.2 Nm. The variation of torque in this weld is again the highest of all 23 mm thickness welds, with a maximum value of 218.1 and minimum value of 183.6, giving a variance of 34.5 Nm across the weld.

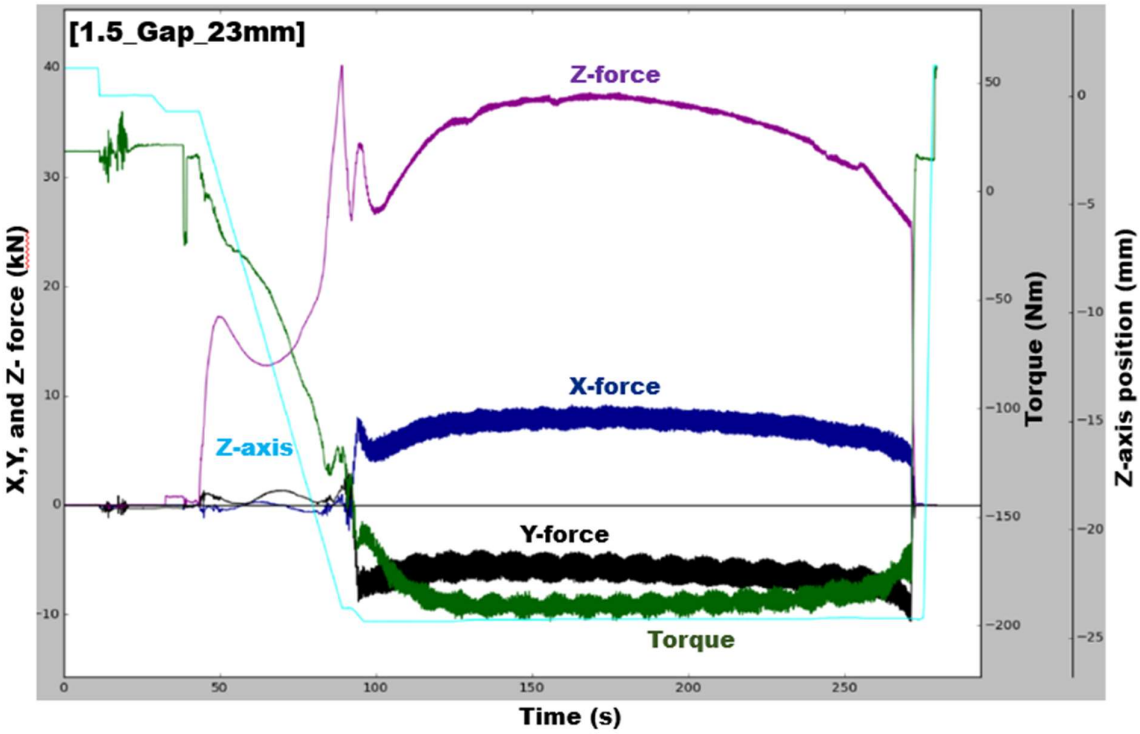

Figure 47: 1.5_Gap_23mm forces and torque

The 2_Gap_23mm weld is again producing a sound cross-section but showing loss of definition and robustness of the TMAZ and this is progressively more noticeable by the end of the weld. In the macrographic photos, Figure 48, the lack of material volume at the top of the weld is noticeable by the beginning of the weld, is corrected slightly in the middle, and again sagging by the end of the weld.

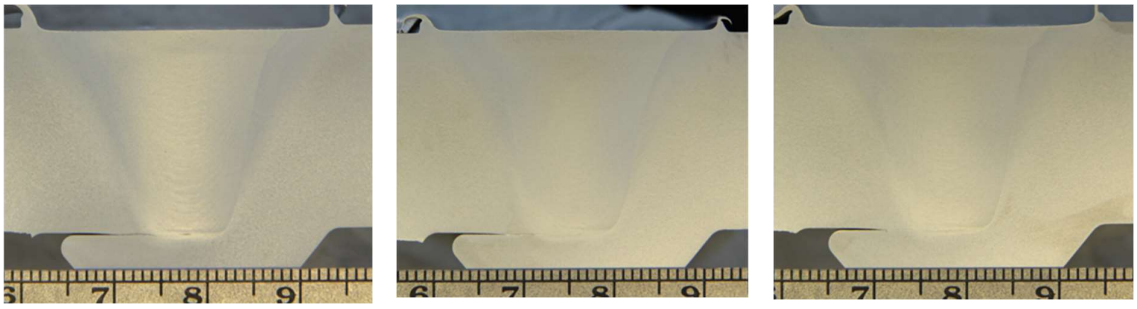

(a) **(b)** **(c)**

Figure 48: : 2_Gap_23mm weld macrography at (a) start, (b) middle, and (c) end

The forces continue in the same trends as the gaps grow larger. The X-force has again dropped to an average value of 6.6 kN, Y-force has increased to an average value of 11.2

kN, and Z-force showing a lower max value of 35.1 kN. The torque has lowered to an average value of 205.8 Nm, as can be seen in Figure 49.

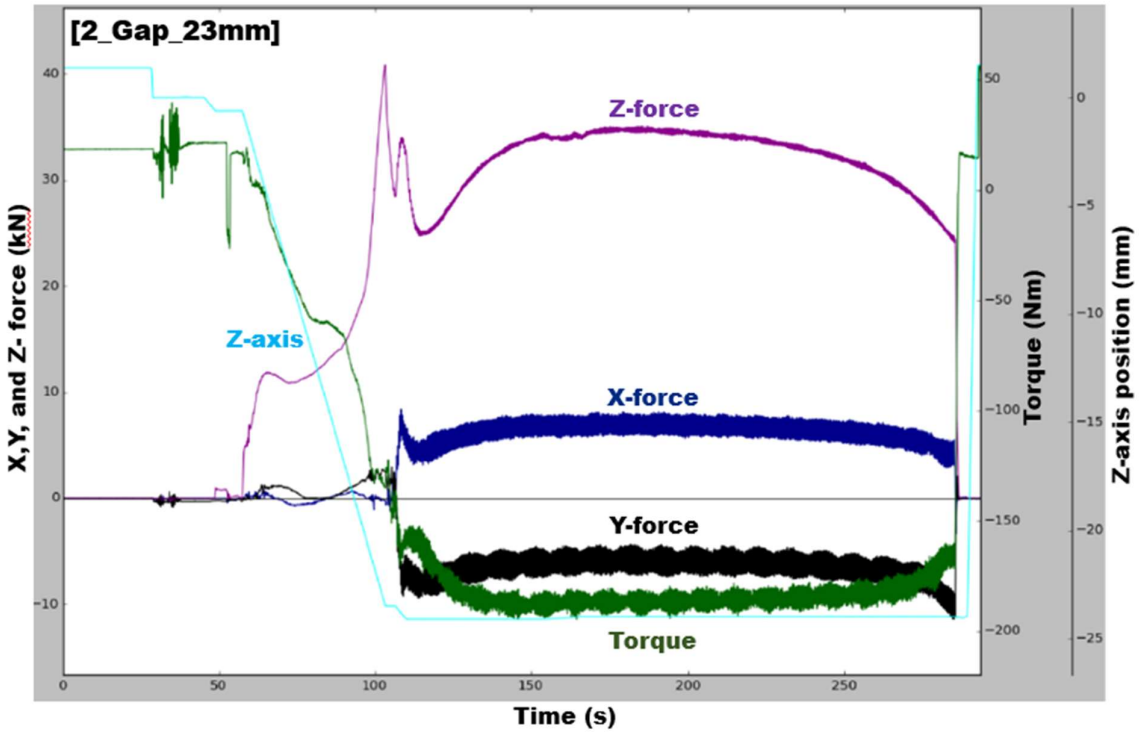

Figure 49: 2_Gap_23mm forces and torque

For the 3_Gap_23mm weld, there is a void visible on the AS of the NZ in the beginning and end of the weld, but not in the middle as can be seen in Figure 50. The void is largest at the end of the weld. This correlates with the surface defects, discussed in section 4.1.4, which were visible on this weld. In the presence of these voids, it can be seen that there is little to no definition or color change in the area of the TMAZ on that side of the weld.

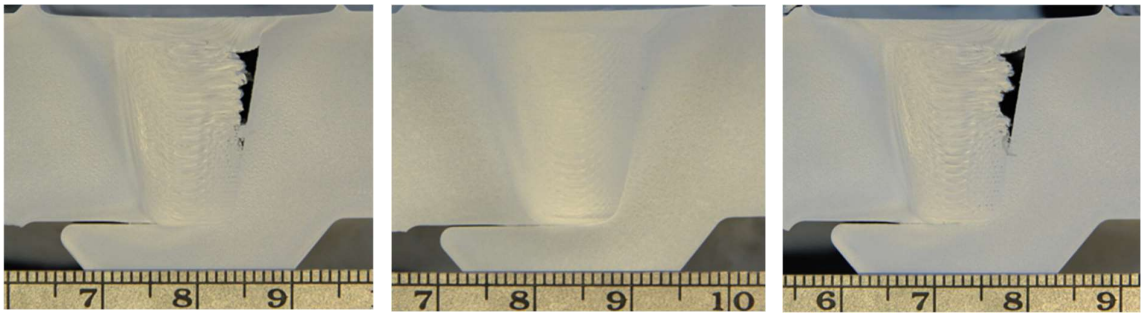

(a) **(b)** **(c)**

Figure 50: 3_Gap_23mm weld macrography at (a) start, (b) middle, and (c) end

The forces in the 3_Gap_23mm weld, shown in Figure 51, are showing signs of instability. The X-force makes a large decrease, from the previous weld to an average value of 4.1 kN. The Y-force makes an increase to an average value of approximately 13.2 kN and makes an uncharacteristically sharp decrease in the center of the weld before increasing again at the end of the weld. The behavior of the Z-force line is typical, but the maximum value has decreased significantly to a value of 27.4 kN. The torque output has decreased

to an average value of roughly 188.7 Nm and shows the largest oscillations of the 23 mm thickness welds. The torque value increases to a maximum value of 203.5 Nm at the center of the weld before dropping significantly to 160.8 at the end of the weld. This is the largest variation in torque of any of the 23 mm thickness welds at 42.7 Nm across the weld.

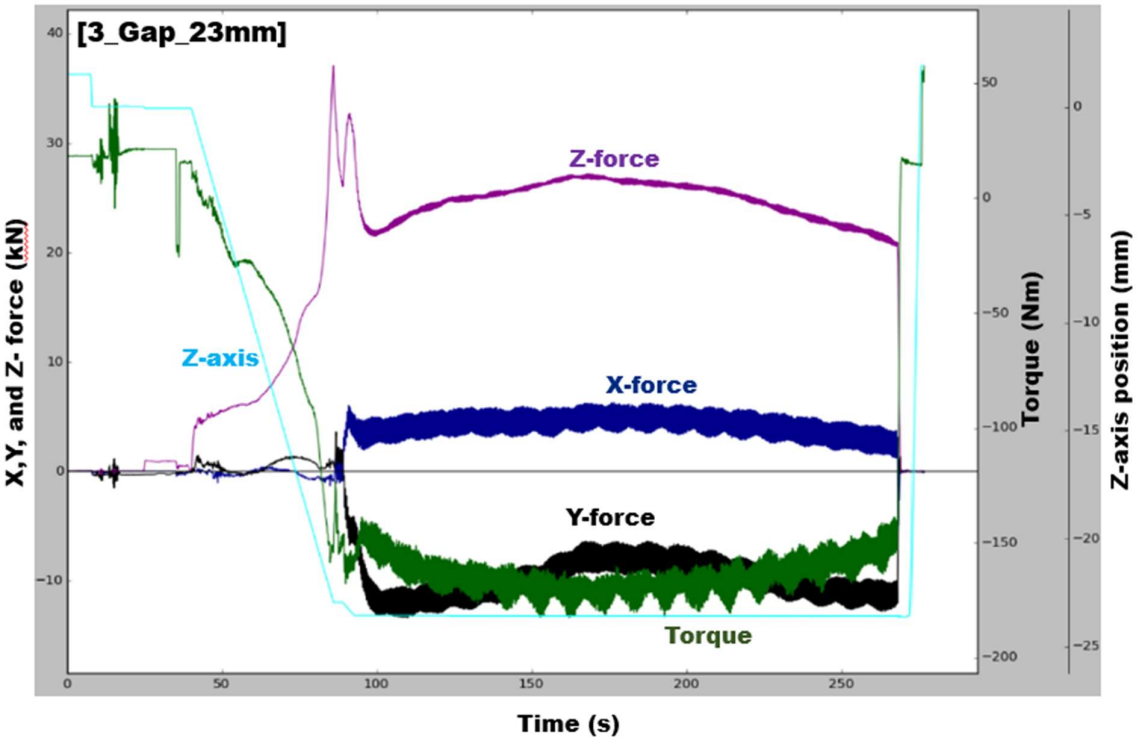

Figure 51: 3_Gap_23mm forces and torque

4.2.4 23 mm welds discussion

Overall, the forces and torques showed similar trends to that of the 17 mm thickness welds. As the gaps grow larger, the X-force, Z-force, and torque are reducing while the Y-force is rising. The variation of the average resulting forces and average torque across the progression of gap levels for the 23 mm thickness welds can be seen in Figure 52.

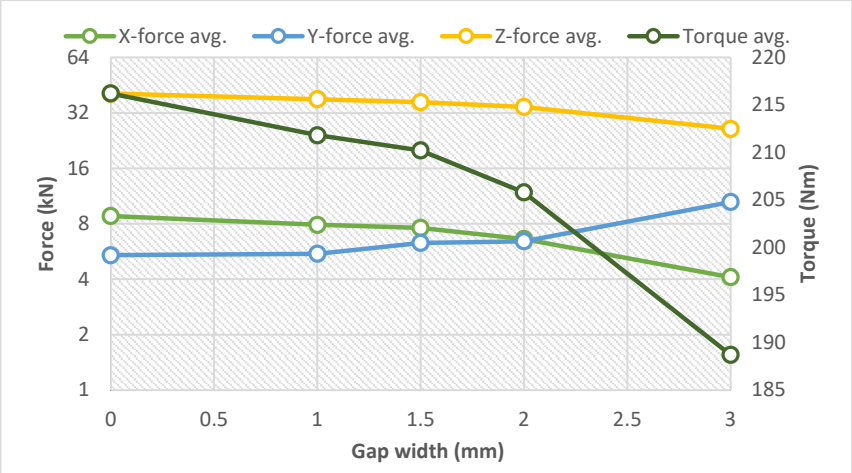

Figure 52: Average forces and torque for 23 mm weld thickness

The graphical output for the 23 mm welds shows typically smoother lines. The variance of the lines is on par with, or higher than that of the 17 mm welds, but more controlled. There are a few possible explanations for this. The process parameters may be better suited for this thickness of weld. There was extra clamping added to the center of the welds to combat some bowing experienced from heat stress from the previously done 17 mm welds, as discussed, and shown in section 3.2.2. Also, the fact that the profiles are already rigidly held together from the weld on the underside could be responsible for more controlled responses in regard to the forces and torque.

Throughout the 23 mm thickness welds the X-force tends to start low, increase to a point near the center, and then decrease again. This follows the pre-weld measurements from section 4.1.1, as the gap measurements were reduced in the center, and wider on the ends near the spacers. The reduction of the gap in the center is offering more resistance, causing the forces in the X direction to increase. The torque values are showing a similar response to the X-forces. The Y-forces are showing an opposite response to the gaps shrinking near the center of the welds. They tend to start high, normalize to a slightly lower value, and they rise again at the end.

In trying to draw a conclusion between the graph and the macrographic images for the 3_Gap_23mm weld, the anomaly that stands out is the sharper than usual decrease in the Y-force near the center of the weld before rising again at the end. This correlates to what is seen in the macrographic examination as this weld experienced voids on either end but not in the center. The graphs for all of the other welds do not show anything similar to this, as they all have fairly constant trends in regard to their forces. The increase in torque near the center of this weld is more extreme than the other welds but is a smoother increase than that of the spike in the Y-force. As mentioned previously, for the 23 mm thickness welds, the Y-force is typically lowering near the center of the welds, where the pre-weld measurements were the lowest. This seems to indicate that the Y-force value is showing a distinct and immediate response to changes in the width of the gap. The reasoning for this is not completely understood, but it can be theorized that the smaller gap increased the frictional heat generation which resulted in softened material and a less rigid lateral force response felt from the side rail pressure.

4.3 Tensile

The results of the tensile tests are presented in this section followed by a discussion.

4.3.1 Tensile Results

The most common region in which the fracturing occurred, for both the 17 mm and 23 mm weld thicknesses, was through the HAZ. This occurred in 25 of the 30 specimens tested. It was typical to see visible yielding in the HAZ on both the AS and RS of the welds before fracturing. All four of the 0_Gap_23mm specimens had the fracture occurring diagonally from the top of the HAZ and through the base material. It is thought that this type of fracture starts in the base material and moves in to the HAZ, but without further analysis this is uncertain. The fracture occurred on the RS of the weld in all but one specimen. In the case of the 1_Gap_23_No5 specimen, the fracture occurred in the AS of the weld and through the base material. In Figure 53, 23 mm weld thickness examples are shown of the typical HAZ fracture, the typical fracture through the base material, and the outlying example of the AS fracture through the base material.

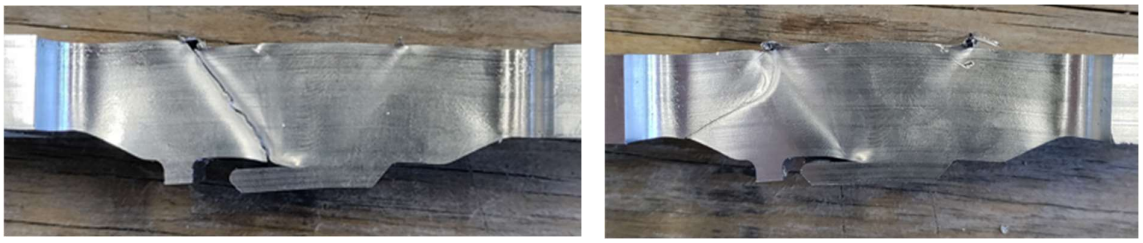

(a) (b)

(c)

Figure 53: 23 mm weld thickness fractures in (a) HAZ on RS, (b) top of HAZ through base material on RS, and (c) top of HAZ through base material on AS

When compared by gap width, the average UTS of the 17 mm thickness welds was higher than their 23 mm counterparts. This comparison can be seen in Figure 54. The 0 mm gap welds had the highest average UTS for both weld thicknesses. The 2 mm gap had the lowest average UTS for the 17 mm thickness welds with a reduction of 3.0 MPa from the 0 mm gap weld average. The 1.5 mm gap had the lowest average UTS for the 23 mm thickness welds with a reduction of 2.0 MPa from the 0 mm gap weld average.

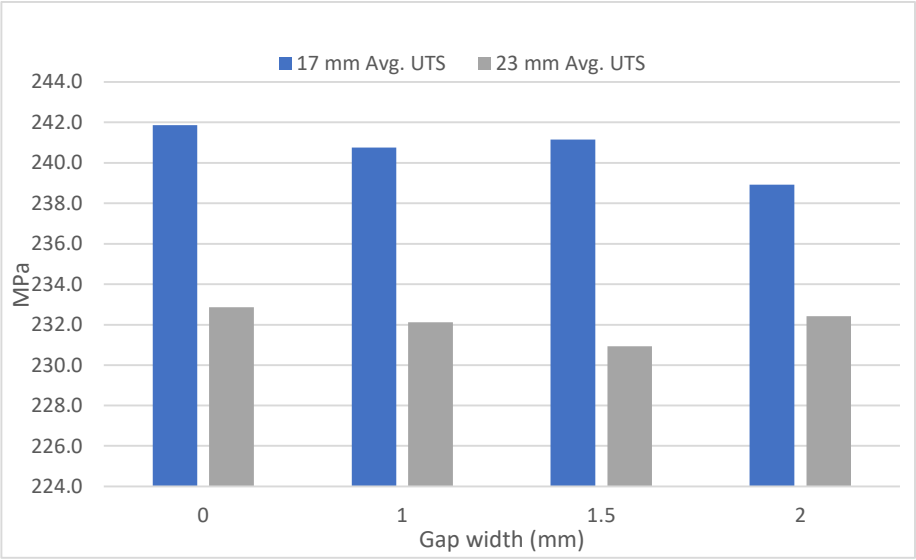

17 mm welds			23 mm welds		
Gap Width	Avg. UTS (MPa)	Std. Dev.	Gap Width	Avg. UTS (MPa)	Std. Dev.
0 mm	241.9	0.258	0 mm	232.9	0.377
1 mm	240.8	0.529	1 mm	232.1	0.305
1.5 mm	241.2	0.315	1.5 mm	230.9	0.178
2 mm	238.9	0.346	2 mm	232.4	0.208

Figure 54: Average UTS comparison across the gap widths

4.3.2 Tensile discussion

The tensile specimens were taken from a region of the weld that is located from 520mm into the weld length and ending at 830 mm into the weld length. In this case, the FSW process has been welding in the presence of a gap for a substantial distance before reaching the area where the specimens are extracted from. This gives an understanding of how the UTS of a FSW responds when encountering gaps, which may result from a curve or twist in a longer extruded profile, which cannot be completely countered with clamping force but can be forced into relative compliance with local deviations of less than 1-meter in length.

After examining the tensile specimens, post-fracture, all specimens showed signs of horizontal bowing within the gauge length in the area of the weld after being stressed vertically. It is unclear if this is due to the nature of the geometry within the cross-section of the specimens or residual stresses held within the welds. Figure 55 shows a comparison of a post-fracture specimen with a straight, untested specimen. Separation can be seen just outside of the width of the weld root, where the two profiles are in contact but unwelded. This is mentioned in this thesis to mark it as an observed phenomenon during the testing progress as well as for any inaccuracies these additional forces may cause towards the results.

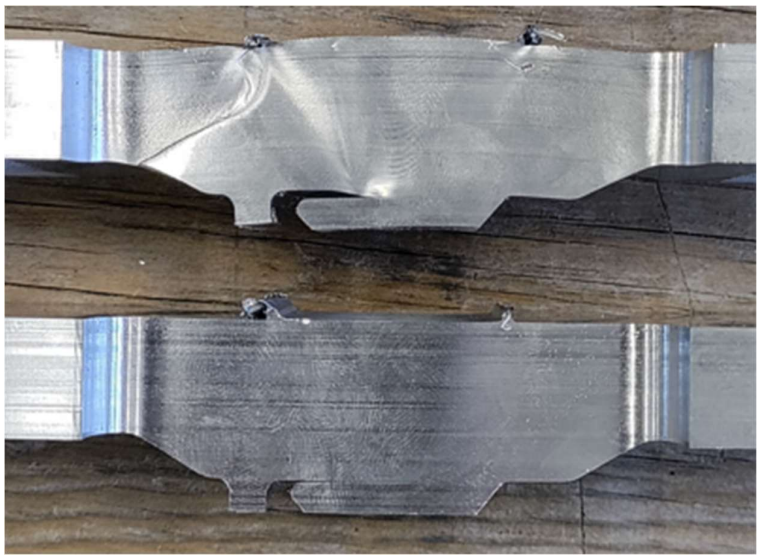

Figure 55: Horizontal bowing in specimen after testing

The FSW process handled the welding gaps with minimal loss of UTS when compared to the baseline gapless weld. Table 12 shows each weld and its % of reduction in UTS when compared to the 0_Gap weld in the same thickness. As mentioned, and shown in the previous section, all of the 0_Gap_23mm specimens fractured through both the HAZ and base material. If this fracture does start in the base material and move to the HAZ, as it is thought to, then that signifies a failure in the geometry as a weak point and not the weld. This has implications for the accuracy of the UTS calculation of the 0_Gap_23mm welds and the UTS % reduction of the 23 mm thickness welds, as shown in the table below. This is because the UTS is calculated with a cross-sectional thickness of 22 mm and the specimen is failing at a shallower depth within the cross-section.

Table 12: Percentage of UTS reduction from gapless welds

17 mm welds		23 mm welds	
Gap Width	UTS reduction from gapless weld (%)	Gap Width	UTS reduction from gapless weld (%)
0 mm	X	0 mm	X
1 mm	0.46	1 mm	0.32
1.5 mm	0.29	1.5 mm	0.83
2 mm	1.22	2 mm	0.19

When welding through a gap, the assumption is that the strength of the weld should continuously decrease as the weld progresses towards the end. The weld is constantly losing material as it fills the vacant area within the gap as well as material lost due to flash. The UTS values from the 17 mm weld thicknesses show that is not necessarily true, as can be seen in Figure 56. The 1- and 2-mm gap welds do lose strength continuously towards the end of the weld, but the 1.5 mm gap has a higher tensile strength in sample number 7 than it does in sample number 6. The 23 mm thickness weld's UTS values also varied throughout out the progression of the weld. The commonality between the 17 and 23 mm weld thicknesses is that, outside of the gapless weld, the sample taken nearest to the end where the spacer is located always tested with the lowest UTS value.

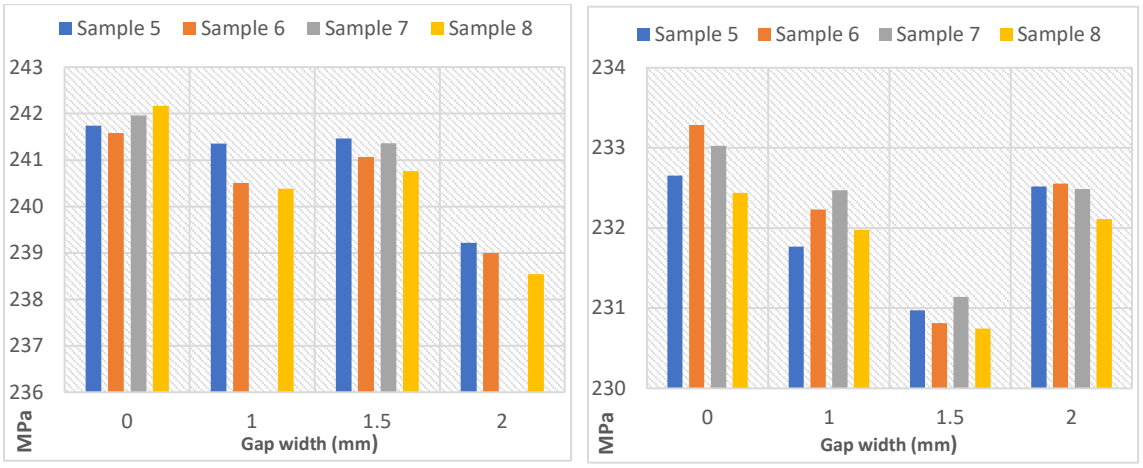

(a) **(b)**

Figure 56: Progression of UTS within each gap width for (a) 17 mm and (b) 23 mm weld thicknesses

It can be seen that the 2_Gap_23mm welds have consistently higher UTS values than that of the 1_Gap_23mm and 1.5_Gap_23mm welds. After searching through the macrographic examinations and forces and torque graphs, no indications are identified in this area of the welds which would provide a clear answer as to why this is. In the progression of these three welds, the established trends of increasing Y-force and decreasing X-force, Z-force, and torque are maintained. The macrographic examination of the end of each weld shows no discernable traits within either of the three welds which would indicate that the 2_Gap_23mm is the stronger weld. All three welds show similar volumetric losses in the shoulder affected zone and the 2_Gap_23 mm welds shows signs of less heat generation

within the weld with less defined TMAZ and HAZ zones visible. The UTS performance of the 2_Gap_23mm is, however, a promising sign towards the successful welding of 3mm gaps and possibly wider. The minimal loss in UTS throughout the experimentation points to the ability of the FSW process, with adjustments made, to handle wider gaps at these weld thicknesses. This will be discussed further with implications towards future work.

5 Conclusion

Experiments were conducted to study the effect that gaps of 1, 1.0, 1.5, 2.0, and 3.0 mm have when FSW 6082-T6 aluminum alloy. The experiments were performed on hollow extruded profiles with welding thicknesses of 17 and 23 mm and length of 1-meter. Discussed within this thesis are observations made during welding, the graphical display of the forces and torque during the welding process, the subsequent macrographic examinations of weld cross-sections, and tensile tests taken from the second half of the weld. The findings are as follows:

- The macrographic examination showed sound, defect free welds in the 1.0, 1.5, and 2.0 mm gap welds.
- The FSW process, as used in this experimentation, was unable to successfully weld through a 3.0 mm gap. The 17 mm thickness weld experienced voids on the AS of the weld, and the 23 mm thickness weld experienced voids on the AS of the weld as well as surface lack of fill defects. The 3.0 mm gap welds were therefore unable to be used for tensile testing.
- The tensile testing results showed that the gaps reduced the UTS of the welded specimens minimally when compared to the gapless weld. In the 17 mm thickness welds the 2.0 mm gap produced the lowest average UTS value, but only 1.22% reduced from the gapless weld. In the 23 mm thickness welds the 1.5 mm gap produced the lowest average UTS value, but only 0.83 % reduced from the gapless weld.
- In the 23 mm weld with a 2.0 mm gap, the average UTS was higher than that of the 1.0 and 1.5 mm gaps. The UTS was 0.19 % reduced from the gapless weld

5.1 Future work

This study reached a number or conclusions regarding the effects that gaps have on the FSW process for thick wall thickness welds. With the observations made during the experiments, combined with information in the related literature reviewed during the course of this thesis, there is opportunity for further study and experimentation:

- This work can be repeated with some alterations to the experimental setup to see if success can be reached with a 3mm gap or improvements made to the UTS of the other gaps. This can be in the form of additional clamping or tack welding to reduce vibration and movement between profiles or adjusting weld parameters. As mentioned in the literature, success has also been found in FSW of gaps with higher tilt angle, using a threaded cylindrical pin, and with strips of compensating material added.
- Welding profiles of longer than 1-meter in length and comparing results.
- Study the extruded profile tolerances and determine clamping forces required in 12-meter-long profiles to ensure gaps which the FSW can manage

6 References

[1] Mazzolani, F.M., *Structural applications of aluminium in civil engineering.* Structural engineering international, 2006. **16**(4): p. 280-285.

[2] Green, J.A., *Aluminum recycling and processing for energy conservation and sustainability*. 2007: ASM International.

[3] Nunez, P., *Long-term sustainability of the aluminium industry.* Aluminium International Today, 2021. **34**(5): p. 15-17.

[4] *Primary Aluminium Production*. [Statistics] 2022 20/01/2022 [cited 2022 26/01]; Available from: https://international-aluminium.org/statistics/primary-aluminium-production/.

[5] Dudin, M., et al., *Modern trends and challenges of development of global aluminum industry.* Metalurgija, 2017. **56**(1-2): p. 255-258.

[6] *Global end use of aluminum products in 2020, by sector*. [Statistics] 2021 25/11/2021 [cited 2022 27/01/2022]; Available from: https://www.statista.com/statistics/280983/share-of-aluminum-consumption-by-sector/.

[7] Rouholamin, M., et al., *Experimental study of roll-formed aluminium lipped channel beams in shear.* Thin-Walled Structures, 2020. **153**: p. 106687.

[8] Çam, G. and G. İpekoğlu, *Recent developments in joining of aluminum alloys.* The International Journal of Advanced Manufacturing Technology, 2017. **91**(5): p. 1851-1866.

[9] Zhang, Y., et al., *Review of tools for friction stir welding and processing.* Canadian Metallurgical Quarterly, 2012. **51**(3): p. 250-261.

[10] Tsarkov, A., K. Trukhanov, and I. Zybin, *The influence of gaps on friction stir welded AA5083 plates.* Materials Today: Proceedings, 2019. **19**: p. 1869-1874.

[11] Wanjara, P., B. Monsarrat, and S. Larose, *Gap tolerance allowance and robotic operational window for friction stir butt welding of AA6061.* Journal of Materials Processing Technology, 2013. **213**(4): p. 631-640.

[12] Georgitzikis, K., et al., *Sustainability aspects of Bauxite and Aluminium.* 2021.

[13] Gándara, M.F., *Aluminium: the metal of choice.* Mater. Tehnol, 2013. **47**(3): p. 261-265.

[14] Gow, N. and G. Lozej, *Bauxite.* Geoscience Canada, 1993. **20**(1): p. 9-16.

[15] Mahinroosta, M., Z. Karimi, and A. Allahverdi, *Recycling of red mud for value-added applications: A comprehensive Review.* 2020.

[16] *Aluminum Facts*. [Government Website] 2022 24/01/2022 [cited 2022 01/02/2022]; Available from: https://www.nrcan.gc.ca/our-natural-resources/minerals-mining/minerals-metals-facts/aluminum-facts/20510.

[17] Cayless, R., *Alloy and temper designation systems for aluminum and aluminum alloys.* 2013.

[18] Mandal, N.R., *Aluminium welding*. 2001: Woodhead publishing.

[19] Kissell, J.R. and R.L. Ferry, *Aluminum structures: a guide to their specifications and design*. 2002: John Wiley & Sons.

[20] Benedyk, J.C., *International temper designation systems for wrought aluminum alloys.* Light metal age, 2010. **67**: p. 3-6.

[21] Kuruveri, U.B., et al., *Surface Modification of 6xxx Series Aluminum Alloys.* Coatings, 2022. **12**(2): p. 180.

[22] Mukhopadhyay, P., *Alloy designation, processing, and use of AA6XXX series aluminium alloys.* International Scholarly Research Notices, 2012. **2012**.

[23] Ding, L., et al., *The natural aging and precipitation hardening behaviour of Al-Mg-Si-Cu alloys with different Mg/Si ratios and Cu additions.* Materials Science and Engineering: A, 2015. **627**: p. 119-126.
[24] Chauhan, K.P.S., *Influence of heat treatment on the mechanical properties of aluminium alloys (6xxx series): A literature review.* Int. J. Eng. Res, 2017. **6**(03): p. 386-389.
[25] Sheppard, T., *Extrusion of aluminium alloys*. 1999: Springer Science & Business Media.
[26] Luksasak, D. *Do you know when to use the indirect extrusion process?* Expert Thoughts 2018 [cited 2022 09/02]; Available from: https://www.shapesbyhydro.com/en/expert-thoughts/do-you-know-when-to-use-the-indirect-extrusion-process/.
[27] Den Bakker, A., et al., *The origin of weld seam defects related to metal flow in the hot extrusion of aluminium alloys EN AW-6060 and EN AW-6082.* Journal of Materials Processing Technology, 2014. **214**(11): p. 2349-2358.
[28] Zhang, C., et al., *Effect of extrusion stem speed on extrusion process for a hollow aluminum profile.* Materials Science and Engineering: B, 2012. **177**(19): p. 1691-1697.
[29] Milkereit, B., et al., *Review of the quench sensitivity of aluminium alloys: analysis of the kinetics and nature of quench-induced precipitation.* Materials, 2019. **12**(24): p. 4083.
[30] CEN, *Aluminium and aluminium alloys. Extruded rod/bar, tube and profiles - Profiles, tolerances on dimensions and form*. 2008, European Committee for Standardization.
[31] Arif, A., et al. *Product defects in aluminum extrusion and its impact on operational cost*. in *The 6th Saudi Engineering Conference, KFUPM, Dhahran, Saudi Arabia*. 2002.
[32] Birol, Y., *The effect of homogenization practice on the microstructure of AA6063 billets.* Journal of Materials Processing Technology, 2004. **148**(2): p. 250-258.
[33] Chahare, A. and K. Inamdar, *Optimization of Aluminium extrusion process using Taguchi method.* IOSR J Mech Civ Eng, 2017. **17**(01): p. 61-5.
[34] Zhang, C., et al., *Optimization of an aluminum profile extrusion process based on Taguchi's method with S/N analysis.* The International Journal of Advanced Manufacturing Technology, 2012. **60**(5): p. 589-599.
[35] Qamar, S.Z., T. Pervez, and J.C. Chekotu, *Die defects and die corrections in metal extrusion.* Metals, 2018. **8**(6): p. 380.
[36] Wang, M.-j., et al., *Simulation of temperature and stress in 6061 aluminum alloy during online quenching process.* Transactions of Nonferrous Metals Society of China, 2014. **24**(7): p. 2168-2173.
[37] Olson, M., et al., *Characterisation of residual stresses in heat treated, high strength aluminium alloy extrusions.* Materials Science and Technology, 2016. **32**(14): p. 1427-1438.
[38] Hydro. *Joining forces to make the world's longest aluminium bridge a reality*. [News] 2020 [cited 2022 25/02/2022]; Available from: https://www.hydro.com/en/media/news/2020/joining-forces-to-make-the-worlds-longest-aluminium-bridge-a-reality/.
[39] Kristensen, V.B., *Aluminium Bridge Girder Alternative*. 2020, Dr. Techn. Olav Olsen, Statens Vegvesen, Hydro, Leirvik, NTNU: Norway.
[40] Shrivastava, A., M. Krones, and F.E. Pfefferkorn, *Comparison of energy consumption and environmental impact of friction stir welding and gas metal arc welding for aluminum.* CIRP Journal of Manufacturing Science and Technology, 2015. **9**: p. 159-168.
[41] DEFALCO, J., *Friction stir welding vs. fusion welding.* Welding journal, 2006. **85**(3): p. 42-44.
[42] Sidhu, M.S. and S.S. Chatha, *Friction stir welding–process and its variables: A review.* International Journal of Emerging Technology and Advanced Engineering, 2012. **2**(12): p. 275-279.

[43] Mishra, A., *Friction stir welding of dissimilar metal: a review.* Available at SSRN 3104223, 2018.
[44] Sivashanmugam, M., et al. *A review on friction stir welding for aluminium alloys*. in *Frontiers in Automobile and Mechanical Engineering-2010*. 2010. IEEE.
[45] Leon, J.S., G. Bharathiraja, and V. Jayakumar. *A review on friction stir welding in aluminium alloys*. in *IOP Conference Series: Materials Science and Engineering*. 2020. IOP Publishing.
[46] Shah, S. and S. Tosunoglu. *Friction stir welding: current state of the art and future prospects*. in *16th World multi-conference on systemics, cybernetics and informatics, Orlando, Florida*. 2012.
[47] ESAB. *Friction Stir Welding*. [Technical Handbook]; Available from: https://assets.esab.com/assetbank-esab/assetfile/12296.pdf.
[48] Neto, D.M. and P. Neto, *Numerical modeling of friction stir welding process: a literature review.* The International Journal of Advanced Manufacturing Technology, 2013. **65**(1): p. 115-126.
[49] Kundu, J. and H. Singh, *Friction stir welding of AA5083 aluminium alloy: Multi-response optimization using Taguchi-based grey relational analysis.* Advances in Mechanical Engineering, 2016. **8**(11): p. 1687814016679277.
[50] Khan, N.Z., et al., *Analysis of defects in clean fabrication process of friction stir welding.* Transactions of nonferrous metals society of china, 2017. **27**(7): p. 1507-1516.
[51] Cole, E.G., et al., *Stability of the friction stir welding process in presence of workpiece mating variations.* The International Journal of Advanced Manufacturing Technology, 2012. **63**(5): p. 583-593.
[52] Ma, H., et al., *Gap-tolerance control for friction stir butt welding of 2A14 aluminium alloy.* Measurement, 2019. **148**: p. 106915.
[53] Widener, C., B. Tweedy, and D. Burford. *Effect of fit-up tolerances on the strength of friction stir welds*. in *47th AIAA/ASME/ASCE/AHS/ASC Structures, Structural Dynamics, and Materials Conference 14th AIAA/ASME/AHS Adaptive Structures Conference 7th*. 2006.
[54] Shultz, E.F., et al., *Effect of compliance and travel angle on friction stir welding with gaps.* Journal of manufacturing science and engineering, 2010. **132**(4).
[55] Singh, A., V. Kumar, and N.K. Grover, *Influence of tool pin profiles on friction stir welding with a gap for AA6082-T6 aluminium alloy.* Materials Research Express, 2019. **6**(8): p. 086543.
[56] Ji, S., et al., *Vertical compensation friction stir welding of 6061-T6 aluminum alloy.* High Temperature Materials and Processes, 2016. **35**(8): p. 843-851.
[57] Abu–Okail, M., et al., *Production of tailor-welded blanks by vertical compensation friction stir welding technique.* Materials Science and Technology, 2018. **34**(16): p. 2030-2041.

Appendix

Chemical composition of alloy used

Result:

Element	Unit	Result
Si	%	0,95
Fe	%	0,19
Cu	%	0,03
Mn	%	0,49
Mg	%	0,61
Cr	%	<0,01
Ni	%	<0,01
Zn	%	0,01
Ti	%	0,01
Pb	%	<0,01

UTS calculations

Formula used for all calculations is UTS = Max F. / (Width x Thickness)

17 mm thickness welds							
Gap (mm)	Sample #	Max F. (N)	Width (mm)	Thickness (mm)	UTS (MPa)	Fract. Zone	Side
0	5	116035	30	16	241.74	HAZ	RS
0	6	115958	30	16	241.58	HAZ	RS
0	7	116142	30	16	241.96	HAZ	RS
0	8	116242	30	16	242.17	HAZ	RS
1	5	115851	30	16	241.36	HAZ	RS
1	7	115446	30	16	240.51	HAZ	RS
1	8	115383	30	16	240.38	HAZ	RS
1.5	5	115903	30	16	241.46	HAZ	RS
1.5	6	115713	30	16	241.07	HAZ	RS
1.5	7	115852	30	16	241.36	HAZ	RS
1.5	8	115566	30	16	240.76	HAZ	RS
2	5	114828	30	16	239.23	HAZ	RS
2	6	114719	30	16	239.00	HAZ	RS
2	8	114502	30	16	238.55	HAZ	RS

23 mm thickness welds							
Gap (mm)	Sample #	Max F. (N)	Width (mm)	Thickness (mm)	UTS (MPa)	Fract. Zone	Side
0	5	153552	30	22	232.65	BM	RS
0	6	153968	30	22	233.28	BM	RS
0	7	153798	30	22	233.03	BM	RS
0	8	153411	30	22	232.44	BM	RS
1	5	152969	30	22	231.77	BM	AS
1	6	153273	30	22	232.23	HAZ	RS
1	7	153432	30	22	232.47	HAZ	RS
1	8	153103	30	22	231.97	HAZ	RS
1.5	5	152444	30	22	230.98	HAZ	RS
1.5	6	152338	30	22	230.82	HAZ	RS
1.5	7	152555	30	22	231.14	HAZ	RS
1.5	8	152292	30	22	230.75	HAZ	RS
2	5	153464	30	22	232.52	HAZ	RS
2	6	153486	30	22	232.55	HAZ	RS
2	7	153440	30	22	232.48	HAZ	RS
2	8	153192	30	22	232.11	HAZ	RS

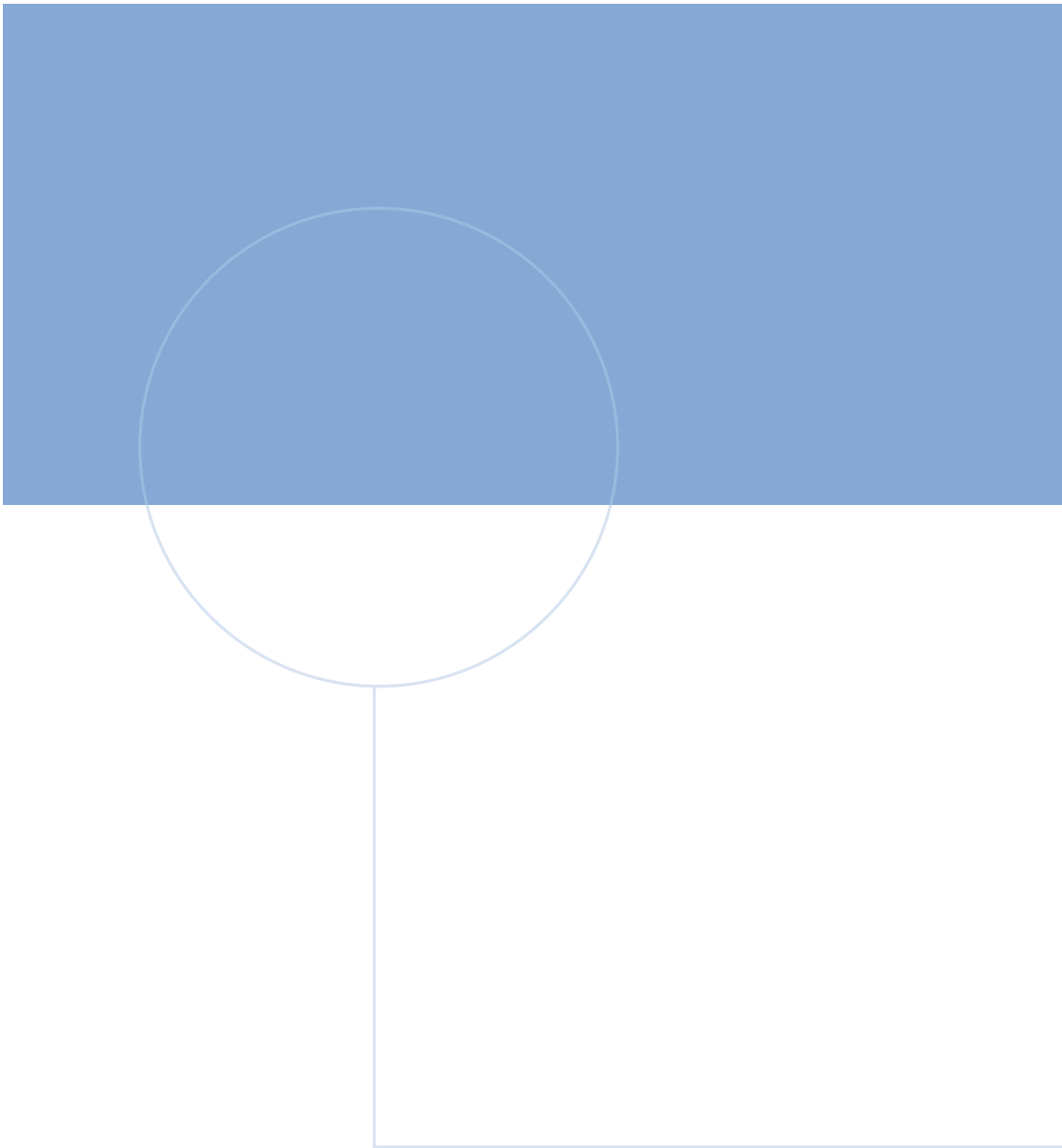

NTNU

Norwegian University of
Science and Technology